AN ABSTRACT OF THE THESIS OF

Matthew T. Smith for the degree of Master of Science in Civil Engineering presented on June 20, 2007.
Title: Investigation of the Behavior of Diagonally Cracked Full-Scale CRC Deck-Girders Injected with Epoxy Resin and Subjected to Axial Tension

Abstract approved:

_____

Christopher C. Higgins

Article 1: Behavior of Epoxy Injected Diagonally Cracked Full-Scale CRC Deck-Girders.

Many cast-in place reinforced concrete deck-girder bridges (RCDG) remain in the national inventory and exhibit diagonal cracking. Epoxy injection has been in use for several decades as a method for sealing diagonal cracks, but the effects on girder behavior have not been validated. Much of the existing data regarding performance of members injected with epoxy have been gathered through testing of reduced-scale specimens. This investigation reports structural responses of five full-scale RCDG specimens constructed to reflect mid-twentieth century proportions and details. Specimens were loaded to produce diagonal cracks, injected with epoxy under varying degrees of axial tension and service loading, and tested to failure. The experimental results indicate that epoxy injection produced minimal capacity increase, increased crack

re-initiation loads, and reduced stirrup serviceability stresses compared to original performance and the control specimen. The addition of cyclic live loading during injection and curing of epoxy produced variable pressures within the crack volume and also produced small bubbles within the epoxy matrix. These bubbles did not reduce performance for the loading considered.

Article 2: Investigation of the Effects of Imposed Axial Tension on Diagonally Cracked Full-Scale CRC Deck-Girders.

Many cast-in place reinforced concrete deck-girder bridges (RCDG) remain in the national inventory and are exhibiting significant diagonal cracking. Current codes for rating and evaluation of bridges permit analysts to neglect temperature and shrinkage effects when calculating load ratings for bridge components with well distributed reinforcement. The proportions and details of 1950's vintage bridges are unlikely to be considered well detailed, and existing research regarding the performance of members subjected to axial tension is insufficient. Seven full-scale reinforced concrete specimens were constructed and tested to reflect mid-twentieth century proportions and detailing, including light shear reinforcement and straight flexural cutoff details. Specimens were loaded under combined axial tension and transverse forces. Results indicate that axial tension and flexural cutoffs reduce member capacity and stiffness and methods for predicting capacity were compared.

Investigation of the Behavior of Diagonally Cracked Full-Scale CRC Deck-Girders Injected with Epoxy Resin and Subjected to Axial Tension

by

Matthew T. Smith

A THESIS

submitted to

Oregon State University

in partial fulfillment of

the requirements for the
degree of

Master of Science

Presented June 20, 2007
Commencement June 2008

Master of Science thesis of Matthew T. Smith presented on June 20, 2007.

APPROVED:

_____

Major Professor, representing Civil Engineering

_____

Head of the Department of Civil, Construction, and Environmental Engineering

_____

Dean of the Graduate School

I understand that my thesis will become part of the permanent collection of Oregon State University libraries. My signature below authorizes release of my thesis to any reader upon request.

_____

Matthew T. Smith, Author

ACKNOWLEDGMENTS

This research was funded by the Oregon Department of Transportation and Federal Highway Administration and overseen by research coordinator Mr. Steven Soltesz. All epoxy resins were donated by Bruce Jackson, BASF sales manager. Equipment and technical support was provided by Toni Kasparek of Williams Form Engineering, Portland, Oregon. The help of these individuals was greatly appreciated. The author would also like to thank all of the graduate and undergraduate team members for their assistance in experimental testing and data reduction. The findings and conclusions are those of the authors and do not necessarily reflect those of the project sponsors or the individuals acknowledged.

CONTRIBUTION OF AUTHORS

Dr. Christopher Higgins and Daniel Howell assisted with testing, data collection and data interpretation. Dr. Higgins also assisted with the writing and organization of this manuscript.

TABLE OF CONTENTS

TABLE OF CONTENTS (Continued)

LIST OF TABLES

LIST OF FIGURES

LIST OF FIGURES (Continued)

General Introduction

A large number of cast-in place reinforced concrete deck-girder (RCDG) bridges remain in the national inventory and are reaching the end of their originally intended design lives. Some states, like Oregon, experienced a building boom of RCDG bridges during the 1950s and 1960s as the interstate highway system was expanded. Field inspections in Oregon identified nearly 500 of these bridges as exhibiting varying degrees of diagonal-tension cracking in the girders and bent caps. Insufficient reinforcing and poor flexural detailing, increasing service load magnitudes and volume, and temperature or shrinkage strains may contribute to diagonal cracking of bridge components.

Epoxy injection is a procedure frequently performed on diagonally cracked bridge components. The injection method is cheap and simple to apply, and has been in use for several decades. However, the effectiveness of epoxy injection to restore or improve RCDG behavior and capacity has not been validated. Additionally, rating and evaluation of existing bridges has begun to move toward the AASHTO-LRFR approach, which states that temperature and shrinkage effects may be ignored when calculating load ratings for bridge components with well distributed reinforcement. It is unlikely that 1950's vintage bridge girders with straight-bar cutoffs in flexural tension regions and lightly reinforced for shear would be considered as meeting such criteria. Research was undertaken on large-size realistically proportioned girders to investigate the interaction of axial tension and epoxy injection on girder behavior.

Behavior of Epoxy Injected Diagonally Cracked Full-Scale CRC Deck-Girders

Matthew Smith, Daniel Howell, and Christopher Higgins

American Concrete Institute Structural Journal

P.O. Box 9094

Farmington Hills, MI 48333-9094

To be published

Introduction and Background

A large number of cast-in place reinforced concrete deck-girder (RCDG) bridges remain in the national inventory and are reaching the end of their originally intended design lives. Some states, like Oregon, routinely constructed RCDG bridges during the 1950s and 1960s, as the interstate highway system was expanded. In 2001, the Oregon Department of Transportation (ODOT) identified nearly 500 of these aging bridges as exhibiting varying degrees of diagonal-tension cracking in the girders and bent caps. Diagonal cracks may be caused by insufficient reinforcing and poor flexural detailing, increasing service load magnitudes and volume, and temperature or shrinkage strains. Diagonal cracks can expose the embedded reinforcing steel to chlorides, moisture, and oxygen that can initiate deterioration and corrosion, thereby causing the structure to weaken. Many repair methods exist that can seal diagonal cracks and possibly restore or increase capacity, such as externally bonded steel and carbon fiber, internal and external stirrups, ferrocement, cement grouting and epoxy injection. Of these methods, epoxy injection has been in use for several decades.

The application of epoxy resin for highway maintenance began during the early 1950's. At the forefront of epoxy material testing was the California Division of Highways Materials and Research Department (Rooney, 1963). Studies utilizing small-sized plain concrete prisms demonstrated that the bond strength of properly applied epoxy was greater than that of the concrete tensile strength (Tremper, 1960). Rupture occurred in the concrete and not in the adhesive bond layer irrespective of the loading conditions (shear,

flexure, or tension). Some of the first uses for epoxy in highway maintenance were patching of damaged roadways and securing reflective traffic markers. Early applications of epoxy injection were performed with a grease gun and were found through observation to improve plate bonding for expansion joints.

As epoxy materials became more widely used, researchers began to investigate the effects of epoxy injection on reinforced concrete members. Early tests to evaluate the performance of epoxy injected reinforced concrete beams were performed by Chung (1975). Each of the three beam specimens in this study measured 125 x 200 mm (5 x 8 in.) with a clear span of 2754 mm (9 ft). Longitudinal and transverse reinforcement were provided, and each specimen was loaded to failure and then injected with epoxy resin. Chung observed that epoxy restored the capacity and integrity of the failed specimens. Another study conducted by Popov and Bertero (1975) examined the behavior of full-scale and half-scale reinforced concrete specimens injected with epoxy and exposed to reversed cyclic loading. The steel detailing and member proportions were typical of large-sized, short-span cantilevers and beam-column sub assemblages for buildings. Complete hysteretic loops were recorded for each of the three specimens in the study, which characterized the cyclic behavior of the injected specimens. They observed that epoxy injection improved the original strength of the specimens but exhibited reduced overall stiffness. At locations where severe rebar-concrete bond degradation occurred, the epoxy did not perform as well. Additional research by Chung (1981) noted that epoxy

injection of small 200 x 300 x 2000 mm (7.9 x 11.8 x 78.7 in.) reinforced concrete beams was not an effective means to restore or improve rebar-concrete bond performance.

Basunbul *et al.* (1990) compared several repair methods for reinforced concrete beams, one of which was epoxy injection. Nine epoxy injected specimens measuring 150 x 150 mm (5.9 x 5.9 in.) in cross section and 1250 mm (49.2 in.) long, with longitudinal and transverse reinforcement, were loaded to induce varying degrees of flexural damage. Cracks were injected with epoxy resin and allowed to cure before each specimen was loaded to failure. The loads required to re-initiate cracking were observed to be higher for the injected specimens compared to the original member response.

In more recent years, the effects of environment and fatigue have been included in studies of epoxy injected specimens. Abu-Tair *et al.* (1991) investigated concrete beams reinforced with transverse and longitudinal steel and measuring 205 x 140 mm (8 x 5.5 in.) in cross section with a 2300 mm (90.6 in.) span. Seven specimens were loaded in flexure to failure and then injected with epoxy resin. Upon reloading, several of the specimens were tested statically, while others were fatigue loaded with varying magnitudes. Additionally, two of the specimens were soaked in 38 ^{o}C (100 ^{o}F) water to investigate the effect of water absorption on durability and performance. The results of the study indicated that epoxy injection restored the original strength and stiffness of the beams regardless of the loading conditions and the four months of water immersion had insignificant effects.

Only a small fraction of the research performed to date on epoxy injection has incorporated full-scale specimens with realistic steel reinforcing details. No data are available for shear response of epoxy injected CRC girders, and few researchers have investigated loading conditions on the curing and bonding of epoxy resin. Furthermore, reduced-sized specimens may not accurately replicate strain fields and behavior of large reinforced concrete members. Other important issues to consider are in-service loading responses and localized behavioral effects, incorporation of service-induced diagonal cracks, and effects of load and shrinkage strains on epoxy injected member performance.

Research Significance

Many CRC bridges with diagonal cracks remain in service today. Epoxy injection is a widely used technique for remediation of cracked concrete, but the efficacy of the method on structural performance has not been established. Many studies have been conducted to investigate the ability of epoxy injection to restore or improve structural behavior, but most previous research is limited to small-sized specimens. An experimental program was conducted using realistic full-scale bridge girders built to represent typical design and detailing from the mid-twentieth century that are commonly encountered in state transportation agency inventories. Diagonal cracks were produced under static load to

represent in-situ cracks. The girders were then epoxy injected and tested under different loading conditions to determine the effects of epoxy injection on structural performance. Research results will help engineers better understand the behavior of epoxy injected diagonally-cracked CRC girders.

Experimental Program

Test Specimens

Five laboratory specimens were constructed and tested to characterize the behavior and capacity of 1950's vintage CRC deck girders with diagonal cracks after being injected with epoxy resin. Previous work by Higgins *et al.* (2004) identified standard details, materials, and proportions used in 1950's vintage bridge construction. Specimens in the current study used an inverted-T configuration to place the deck in flexural tension. This arrangement is representative of negative moment in high-shear locations near continuous supports such as piers and bent caps. Each specimen had the same geometry measuring 1219 mm (48 in.) overall height, with a stem width of 356 mm (14 in.), and a deck flange 152 mm (6 in.) thick by 914 mm (36 in.) wide. Figure 2.1 illustrates the member proportions and reinforcing steel details. Longitudinal reinforcing steel consisted of ASTM A615 Grade 420 (Gr. 60) bars, and Grade 300 (Gr. 40) stirrups were used for transverse reinforcement. Tension tests were performed to determine the reinforcing steel properties which are summarized in Table 2.1.

Concrete was provided by a local ready-mix supplier for all specimens. The concrete mix design was based on 1950's AASHO "Class A" concrete used in previous research at OSU (Higgins *et al.*, 2003). Specified compressive strength was 21 MPa (3000 psi), which is comparable to the specified design strength in the original 1950's bridges. Actual concrete compressive strengths were determined from 152 x 305 mm (6 x 12 in.) cylinders tested for 28 day and day-of-test strengths in accordance with ASTM C39M/C 39M-05 and ASTM C617-05. Day of test concrete cylinder strengths for each specimen are shown in Table 2.1 The aggregate composition for the mix was reported by the supplier as: 97% passing the 19 mm sieve (3/4 in.), 82% passing 16 mm (5/8 in.), 57% passing 12.5 mm (1/2 in.), 33% passing 9.5 mm (3/8 in.), 21% passing 8 mm (5/16 in.), 9.3% passing 6.3 mm (1/4 in.), 3.0% passing 4.75 mm (#4), 0.6% passing 2.36 mm (#8) and 0.3% passing the 0.075 mm (#200) sieve. The sand composition of the mix was also reported as: 99.7% passing the 6.3 mm sieve (1/4 in.), 96.8% passing 2.36 mm (#8), 59.4% passing 1.18 mm (#16), 44.9% passing 0.600 mm (#30), 17.9% passing 0.300 mm (#50), 3.7% passing 0.150 mm (#100) and 1.7% passing the 0.075 mm (#200) sieve. The coarse aggregate was from Willamette River bed deposits consisting of smooth rounded basaltic rock.

Instrumentation

Internal and external sensors were positioned on the specimens to record the local and global member responses. Strain gages were placed on stirrups located within the critical shear section near midspan. Additional strain gages were mounted to the flexural

reinforcement at midspan in the tension region. Displacement transducers were placed within three regions on each side the beam to measure diagonal deformations. Displacement transducers were also placed on the support centerlines on each end and on both sides. Midspan displacements were measured with string potentiometers. The actual centerline displacement presented in subsequent figures was calculated by removing the support deformations from the overall centerline deformation during each load cycle. Typical instrumentation is illustrated in Fig. 2.1.

Testing Methodology

A simply-supported four-point loading configuration was used with an overall span length of 6604 mm (260 in) from centerline of supports. Force was applied with a hydraulic actuator at a constant rate of 8.9 kN/sec (2.0 kips/sec) and was measured by a 2224 kN (500 kip) capacity load-cell. A spreader beam distributed the applied actuator force to 102 mm (4 in.) wide plates spaced 610 mm (24 in.) symmetrically about midspan. Loading was applied in steps with incrementally increasing load followed by unloading. Load magnitudes increased each cycle by an amount of 222 kN (50 kips). At each load peak, the load was reduced by 10% to minimize creep effects and visible cracks were measured and marked. Three tests were performed on each specimen with the exception of the control specimen, 1-C, which was loaded to failure in a single test. An initial loading sequence, or precrack test, was performed to produce diagonal cracks similar to those observed in field inspections of RCDG bridges and of sufficient size for epoxy injection. A target diagonal crack range of 0.65 mm-1.25 mm (0.025in-0.05in) was

selected based upon the prior work of Higgins *et al.* (2004). When diagonal cracks reached suitable size, the precrack loading cycle was terminated and a baseline test was performed to establish a reference for the specimens in the cracked condition for comparison to the post-injection response. In the final test, all specimens were loaded incrementally to failure.

Injection and Curing Procedures

The epoxy selected was SCB Concresive 1360 produced by Chemrex. This particular resin is a two-part, ultra low-viscosity liquid epoxy. The specified material tensile strength for SCB Concresive 1360 is 55.2 MPa (8000 psi). The surface sealant used was Concresive SPL Paste, which is a two-part, 100% solids epoxy. These two materials are commonly used, are pre-approved for use by several State DOTs, and are representative of similar epoxy materials. All injection materials were provided by local suppliers. Additional installation guidance was provided by qualified contractors to establish a repair protocol that satisfied the manufacturer's installation recommendations. The procedure that was established is summarized below:

The concrete surfaces around the diagonal cracks were cleaned with a wire brush to remove loose particles and dirt. Vacuuming was performed to assure a clean surface area. The crack perimeter was sealed and injection ports were surface mounted every 356 mm (14 in.) or roughly equal to the width of the girder web. The surface epoxy cured for 24 hours before the injection process was initiated. Diagonal cracks were injected starting

from the lowest port working up which allowed for release of entrapped air. “Window” ports were placed on the backside of the beam to serve as a visual aid for assurance of epoxy penetration through the beam web. A specialized injection machine was used to mix the two part liquid epoxy in the manufacturer’s recommended proportions and deliver the mixture into the beam under pressure. This machine is commonly used by contractors performing this work. Each port was injected to a maximum pressure of 690 kPa (100 psi). As liquid epoxy began to seep from the next higher tube, the lower port was capped and the injection nipple moved to the next higher position. Near the top of each diagonal crack, the injection pressure climbed more quickly to 690 kPa (100 psi), and would take longer to dissipate, signaling that there was little available space to pump additional epoxy resin. When the maximum pressure could be maintained, the final port was capped. After injection, all specimens were allowed to cure for at least seven days. A heated plastic enclosure was placed around the specimen to ensure that temperatures were maintained above 4.5^{o} Celsius (40^{o} Fahrenheit). Thermocouples outfitted with data loggers were placed into a small void cast into the end of the specimens and on the exterior to record temperatures and ensure the specified curing conditions.

Specimen Variables

To simulate the effects of different stress conditions, each specimen was subjected to a distinct loading scenario during the injection and curing phases. Specimen 2-EC was injected and cured with no applied loads other than specimen self-weight. Simulated superstructure dead load was applied to specimen 3-ED before epoxy injection. A total

load of 356 kN (80 kip) was applied to induce a service level dead load shear of 178 kN (40 kip). This shear magnitude is representative of an interior girder for a typical 1950's vintage 3-span continuous CRC deck-girder bridge having 15.2 m (50 ft) spans and a uniform dead load of 23.3 kN/m/girder (1.6 kip/ft/girder). Varying live load stress was applied to specimen 4-EL in addition to the superstructure dead load. The live loading was representative of average shear magnitudes produced by ambient traffic and a fully-loaded Type 3-3 unit truck having 5 axles and a gross vehicular weight of 356 kN (80 kip) moving across a similar bridge as that for specimen 3-ED using realistic shear distribution factors developed by Potisuk and Higgins (2007) from field studies. Force was applied at 0.3 Hz with an amplitude of 160 kN (36 kips) and a mean of 463 kN (104 kips). This loading represents the maximum girder shear caused by the dead load of the bridge and the truck live load with impact, as well as a minimum force resulting from hogging due to live load moving onto an adjacent span. The fifth specimen, 5-EA, had simulated locked in drying and thermal shrinkage strains induced by applying a uniform tension load to the specimen. The axial load was applied to a level of approximately 890 kN (200 kip) before the initial precrack transverse loading cycles began. The axial load was held at a constant magnitude of 645 kN (145 kip) during the injection and curing phases, and then returned to 890 kN (200 kip) for the post-injection failure loading. For additional detail on the axial force application and loading protocol, please refer to Chapter 3.

Experimental Results

The performance of the epoxy injected specimens was evaluated through the shear-deflection responses, flexural and shear reinforcement demands, and crack deformations. The data collected from the three phases of testing were compared to assess the local and global responses before and after injection. Results were also compared with an otherwise similar un-injected specimen.

The material properties for concrete and steel varied from specimen to specimen, preventing direct comparisons between test specimens. In a previous study, a computer program called Response 2000 (R2K) (Bentz, 2000), which utilizes Modified Compression Field Theory (MCFT), was used to predict shear capacity for a series of 31 otherwise similar full-size CRC specimens. The program predicted capacity within 0.98 of actual with a coefficient of variation under 8% (Higgins *et al.* 2004). R2K was used to estimate the inherent capacities of the epoxy-injected specimens in their unaltered state as well as the strength of the control specimen. The predicted shear strengths are summarized in Table 2.2. On average, the epoxy-injected specimens provided slightly larger shear capacities than predicted, ranging from 1.02 to 1.20 for specimens 2-EC and 5-EA, respectively. The total applied shear is a combination of the experimental load applied by the actuator and the specimen dead load comprised of the self-weight associated with the failure section. All specimens exhibited shear-compression failures. The specimens with the largest improvement over predicted unaltered shear capacity were specimens 4-EL and 5-EA. These two specimens received the least amount of

epoxy injection in comparison to the other two specimens. Several of the diagonal cracks on 4-EL and 5-EA were too small to inject; consequently, only three major diagonal crack systems were injected on each of these specimens. Specimens 2-EC and 3-ED had more numerous diagonal cracks of sufficient size to inject. Axial load was accounted for in the R2K capacity prediction of specimen 5-EA, however, Chapter 3 discusses this aspect in greater depth as well as compares specimen 5-EA with other similarly axially loaded specimens. In summary, specimen 5-EA exhibited significantly greater strength than predicted, and generally has superior responses over similarly tested axial and epoxy injected specimens.

Midspan shear-displacement responses are shown in Fig. 2.2 and display the overall specimen behavior of the initial, baseline, and post-injection tests. The post-injection response of each injected specimen showed decreased residual deformations and greater stiffness during the initial two or three load steps. As the applied shear magnitudes increased, the specimens began to soften due to new cracking and residual deformations increased. This behavior is especially pronounced in specimen 4-EL. Specimens 3-ED and 4-EL were similar, especially in the service load range indicated in the figures, and both had greater stiffness than specimen 2-EC. The axially loaded specimen exhibited a unique shear-midspan deformation response unlike the other four. The curve has a slender “S” shape as the specimen stiffens and then softens during each load cycle. Figure 2.3 displays the axial load as a function of the applied shear for specimen 5-EA. As the applied shear magnitude increased, the specimen length increased at the level of

the axial apparatus thereby reducing the hydraulic pressure in the axial load actuators, thus reducing the applied axial tension. As the applied shear decreased, the specimen shortened along the axial loading apparatus and the axial tension increased again. Like specimen 4-EL, specimen 5-EA had decreased residual deformations for many of the load cycles and did not begin to soften until near failure. Conversely, the control and precrack tests were softer, showing greater permanent deformation at each higher load step.

Similar behavior to the shear-midspan displacement responses was evident in the post-injection diagonal displacement data shown in Fig. 2.4. All of the post-injection tests for the epoxy specimens had smaller permanent deformations during the initial load steps than did the control specimen in addition to having a greater stiffness. Specimens 3-ED and 4-EL were stiffer than specimen 2-EC, with specimen 4-EL performing slightly better than 3-ED. The largest impacts were again seen in specimen 5-EA which showed significantly improved stiffness and a reduced permanent deformation response. For all the specimens except 4-EL and 5-EA, the north and south diagonal deformations were essentially identical, showing similar stiffness and exhibiting significant diagonal deformation at approximately the same shear magnitude. For the remaining two specimens, however, one side had a substantially larger load at the point where the diagonal deformation first changed slope. This may be a result of the uneven distribution of shear cracks and epoxy resin. For specimen 4-EL, the side with the lower crack re-

initiation load contained fewer diagonal cracks that were epoxy injected. Specimen 5-EA had more active diagonal cracks on the side with the lower cracking shear.

The largest relative influences of epoxy injection were seen in the individual rebar strain, but these effects were highly influenced by the proximity of injected diagonal cracks to instrument locations. The orientation and location of the diagonal cracks produced during precrack and post-injection loading sequences are shown in Fig. 2.5. The location of diagonal cracks that were epoxy injected are also shown. Diagonal cracks that were injected did not reopen during post-injection tests. Instead, new cracks formed adjacent to the injected cracks and propagated at similar angles. Non-repaired cracks tended to propagate along the original paths. Stirrups located near diagonal cracks that were injected had lower strains after injection at otherwise similar shear load. Stirrups located between diagonal cracks or far from cracks that were not injected displayed relatively little change. This behavior was observed for all injected specimens. Diagonal cracks were considered to be "near" the stirrup strain gage if the vertical distance that the crack crossed the stirrup was within the AASHTO calculated development length of the #13 (#4) stirrup. Figure 2.6 shows an example of strains measured for a stirrup located near a diagonal crack and a stirrup located at a distance greater than the development length from a diagonal crack.

The strain behavior depicted in Fig. 2.7 shows the baseline and post-injection stirrup strains at the maximum service load level. In the figure, the baseline strains serving as the

abscissa are plotted against the post injection strains operating as the ordinate. Solid symbols represent stirrup strain gages located near injected diagonal cracks as defined above, while hollow symbols represent stirrup strain gages located away from injected diagonal cracks. The dashed reference line marks the boundary between improved and un-improved behavior. Points above the line had higher strains at the same service load after injection, while the points below the line had lower strains after injection. Most stirrup strains near injected diagonal cracks showed significantly reduced strains after injection, whereas un-injected regions were generally unaffected.

The applied loads required to re-initiate diagonal cracking are portrayed in a similar fashion as seen in Fig. 2.8. The load required to re-initiate diagonal cracking was determined from the applied shear magnitude at the moment the stirrup strain showed an abrupt increase. The pre and post-injection diagonal cracking shears were compared with the precrack diagonal cracking shear as the abscissa and the post-injection cracking shear serving as the ordinate. Injected diagonal cracks required higher applied shear than the original specimen to produce new diagonal cracking. Data above the reference line show that larger shear loads were required, while points below the line required smaller loads to propagate or re-initiate diagonal cracking. Non-injected cracks typically behaved similar to the baseline tests, where stirrup strains began increasing upon application of applied shear.

An additional test was performed on specimen 4-EL to collect data while the specimen was curing and the cyclic service level live loading was being applied. Figure 2.9 shows the deformation range of a representative displacement sensor while Fig 2.10 shows an example of the stirrup strain throughout the curing period. Also shown in Fig 2.10 are the internal and external temperature recordings. The curing time reported by the epoxy manufacturer is seven days at 4 ^{o}C (40 ^{o}F) and 2 days at 25 ^{o}C (77 ^{o}F). The average curing temperature for specimen 4-EL was 10 ^{o}C (50 ^{o}F), which correlates to a curing time of approximately six days. The diagonal deformations for the region containing epoxy injected diagonal cracks showed marked decrease in deformation within 12 hours of injection. Over the next three days, the deformation range decreased by nearly 75%. For a stirrup located in the same section as the example diagonal deformation, the strain range decreased by over 50% within the first 18 hours, but little additional effects were observed for the remainder of the curing process. The stirrup strain was also observed to fluctuate with the external temperature. Diagonal displacement measurements also tended to fluctuate with time, but the mean deformation did not alter significantly.

Discussion

The results of this study indicate that epoxy injection affects the structural behavior of CRC girders. Overall, the most dramatic effects were observed for specimens 3-ED, 4-EL and 5-EA. Specimen 3-ED exhibited a higher capacity compared to the predicted baseline capacity. Specimen 3-ED also achieved higher loads prior to re-initiation of nonlinear response as compared to the epoxy injected control specimen, 2-EC. The dead load

serves to prop the diagonal cracks open allowing for deeper penetration of the epoxy into the cracks. It further allows the epoxy to only carry superimposed live loads and leaves dead load stresses locked into the rebar and concrete. This tends to delay crack re-initiation and forces new cracks to form adjacent to the previously cracked location. This was observed by the reduced stirrup steel demand at injected diagonal cracks for otherwise similar load levels and the formation of new cracks alongside or in-between epoxy injected diagonal cracks. The live load magnitudes, rates, and curing conditions considered in this program for specimen 4-EL did not reduce the effectiveness of the epoxy injection as compared to the specimen with dead load alone. The performance of both specimens was very similar. The cyclic loading may have acted as an internal pumping mechanism that enabled the epoxy to enter and fill finer cracks than either specimen 3-ED or specimen 2-EC. It was observed during the injection process of specimen 4-EL that the epoxy pump pressures built and dissipated in-phase with the actuator loading cycle. The pulsing was also observed when the surface sealant cracked and leaks developed which were then sealed with paraffin wax. The epoxy would be pushed out of the diagonal cracks as the cracks closed upon unloading. Concrete cores measuring 102 mm (4 in.) in diameter were taken from epoxy injected diagonal cracks for both specimens 3-ED and 4-EL. Both cores showed epoxy was well distributed through the cracks and even filled hairline sub-cracks. The core from specimen 4-EL had small visible pores which were evidence of bubble formations likely caused by the internal pumping action due to the working diagonal cracks. Fig. 2.11 shows examples of the porous epoxy matrix observed in specimen 4-EL compared to the solid epoxy matrix

observed in specimen 3-ED. The development of bubbles within the epoxy were not sufficient to diminish the performance of specimen 4-EL compared to specimen 3-ED. It is important to note that the cyclic live loading was representative of loads moving across a typical 15.2 m (50 ft.) span continuous bridge at an approximate speed of 32 kph (20 mph). Additional research is needed to study the effects of highway speeds and load magnitudes simultaneously applied during epoxy injection, and possible lower-range curing temperatures.

The axially loaded specimen, 5-EA, exhibited the most dramatic change between the pre-injection and post-injection response compared to the other specimens. The specimen was injected when an externally applied axial tension was held constant at 645 kN (145 kip), the load magnitude at the end of the of the precrack test. This axial force held the diagonal and vertical cracks open allowing for better penetration of the epoxy similar to specimens 3-ED and 4-EL. Additionally, as the transverse loading was applied, the axial force decreased during testing to a magnitude of 267 kN (60 kip) at failure, resulting in a tension force of 267 kN (60 kip) in the flexural steel and a net compressive force of 378 kN (85 kip) induced into the epoxy injected section. Had the axial load not diminished with increasing transverse load, the specimen may have failed at lower load levels. Response 2000 predicted a capacity of 853 kN (192 kip) for a similar specimen with 890 kN (200 kip) total axial tension force. Reducing the steel yield stress by an amount equivalent to the 267 kN (60 kip) axial tension and applying a 378 kN (85 kip) axial compression force on the section, Response 2000 estimates a shear capacity of 987 kN

(222 kip) which is closer to the observed shear capacity. This situation of loading and curing is representative of a structure with shrinkage or differential temperature strains that are recovered after epoxy injection. The stress recovery (release of restraints at supports for example) produces a post-tensioning effect for the injected specimen, but this beneficial effect could not be relied upon in the field.

Basunbul *et al.* (1990) noticed during their experiments that the cracking loads for their epoxy-injected specimens increased in comparison to the control specimens. They presented a hypothesis that the steel stresses at the location of un-injected cracks will be larger relative to the steel stress at the injected cracks upon reloading. As load is applied, unaltered cracks will have a higher propensity to grow than the injected but the higher steel stresses will help to limit the growth of the fine cracks, thus increasing the cracking load.

Conclusions

Five CRC girders built to reflect the design and construction practice of 1950's vintage RCDG bridges were tested to study the effects of epoxy injection applied to diagonal cracks on structural performance. Specimens were pre-cracked to levels observed in the field, subjected to baseline tests in the cracked condition, injected with epoxy resin, and then tested to failure. The results of the initial cracking, baseline, and post-injection responses were compared. Factors included in the study were dead load, service live load

plus dead load, and externally applied axial tension. Based on the experimental observations, the following conclusions are presented:

- Capacity was only slightly increased by epoxy injection. The largest capacity increases were observed for specimens with the live load and externally applied axial tension (which was due principally to an unintended post-tensioning effect).
- Live loading during injection and curing of epoxy produced dynamic pressure fluctuations during the injection process and pumping of the epoxy within the diagonal cracks. Fine bubbles were identified in the epoxy matrix for cores taken after testing for the specimen with applied live loads, but these bubbles were not sufficient to diminish performance.
- Stiffness was improved and development of residual deformations was delayed by epoxy injection.
- Epoxy injection increased the load level required to form diagonal cracks in the stem.
- Injected diagonal cracks did not reopen, instead new cracks formed adjacent to the original injected cracks.
- Epoxy injection reduced service-level stirrup strains compared to un-injected diagonal cracks. This may reduce bond fatigue thereby slowing or preventing additional crack growth.

REFERENCES

Abu-Tair, A. I., Rigden, S. R., and Burley, E., "The Effectiveness of the Resin Injection Repair Method for Cracked RC Beams," *The Structural Engineer*, V. 69, No. 19, Oct. 1991, pp. 335-341

ASTM C 39/C 39M-05, "Standard Test Method for Compressive Strength of Cylindrical Concrete Specimens," ASTM International, 2005, pp. 21-27.

ASTM C 617-98, "Standard Practice for Capping Cylindrical Concrete Specimens," ASTM International, 2005, pp. 1-5.

Basunbul, I. A., Gubati, A. A., Al-Sulaimani, G. J., and Baluch, M. H., "Repaired Reinforced Concrete Beams," *ACI Materials Journal*, V. 87, No. 4, July-Aug. 1990, pp. 348-354

Bentz, E., Response 2000, University of Toronto, <http://www.ecf.utoronto.ca/~bentz/r2k.htm>.

Chung, H. W., "Epoxy-Repaired Reinforced Concrete Beams," *Journal of the American Concrete Institute,* V. 72, No. 5, May 1975, pp. 233-234

Chung, H. W., "Epoxy Repair of Bond in Reinforced Concrete Members," *Journal of The American Concrete Institute*, V. 78, No.1, Jan.-Feb. 1981, pp. 79-82

Higgins, C., Miller, T. H., Rosowsky, D. V., Yim, S. C., Potisuk, T., Daniels, T. K., Nicholas, B. S., Robelo, M. J., Lee, A-Y., and Forrest, R. W., "Research Project SPR 350 SR 500-91: Assessment Methodology for Diagonally Cracked Reinforced Concrete Deck Girders," Oregon Department of Transportation, Salem, OR, Oct. 2004, 328 pp.

Higgins, C., Farrow, W III, C., Potisuk, T., Miller, T. H., Yim, S. C., Holcomb, G. R., Cramer, S. D., Covino, B. S., Bullard, S. J., Ziomek-Moroz, M., and Matthes, S. A., "SPR 326 Shear Capacity Assessment of Corrosion-Damaged Reinforced Concrete Beams," Oregon Department of Transportation, Salem, OR, 2003, 19 pp.

Popov, E. P., and Bertero, V. V., "Repaired R/C Members Under Cyclic Loading," *Earthquake Engineering and Structural Dynamics,* V. 4, No. 2, Oct.-Dec. 1975, pp. 129-144

Potisuk, T., and Higgins, C., "Field Testing and Analysis of CRC Girder Bridges," *Journal of Bridge Engineering*, ASCE, V. 12, No. 1, Jan.-Feb. 2007, pp. 53-63

Rooney, R. A., "Epoxy Resins as a Structural Repair Material," State of California Department of Public Works Division of Highways, <http://www.dot.ca.gov/hq/research/researchreports/1961-1963/63-23.pdf, Jan. 1963, pp. 15

Tremper, B., "Repair of Damaged Concrete with Epoxy Resins," *Journal of the American Concrete Institute,* V. 32, No. 2, Aug. 1960, pp. 173-182

Table 2.1: Concrete and steel properties. Values are for failure test unless otherwise indicated.

Specimen	Concrete		Reinforcing Steel			
			#13-Grade 300		#36-Grade 420	
	f'c (MPa)	Tensile @ Initial Loading (MPa)	F_y (MPa)	F_u (MPa)	F_y (MPa)	F_u (MPa)
1-C	28.5	3.17 @ 28-day	350	544	477	712
2-EC	36.2	2.8	357	570	492	741
3-ED	28.3	2.6			484	728
4-EL	29.5	2.7			473	694
5-EA	35.5	2.8			492	741

Table 2.2: Specimen experimental summary.

Specimen	V_{intial} (kN)	V_{exp} (kN)	V_{DL} (kN)	V_{app} (kN)	V_{R2K} (kN)	V_{app}/V_{R2K} (kN)	Failure Mode
1-C	N/A	902	16.9	919	954	0.96	Shear-Comp.
2-EC	723	983	20.3	1003	982	1.02	Shear-Comp.
3-ED	778	992	17.2	1009	967	1.04	Shear-Comp.
4-EL	778	1046	16.7	1063	949	1.12	Shear-Comp.
5-EA	778	1112	18.4	1130	943	1.20	Shear-Comp.

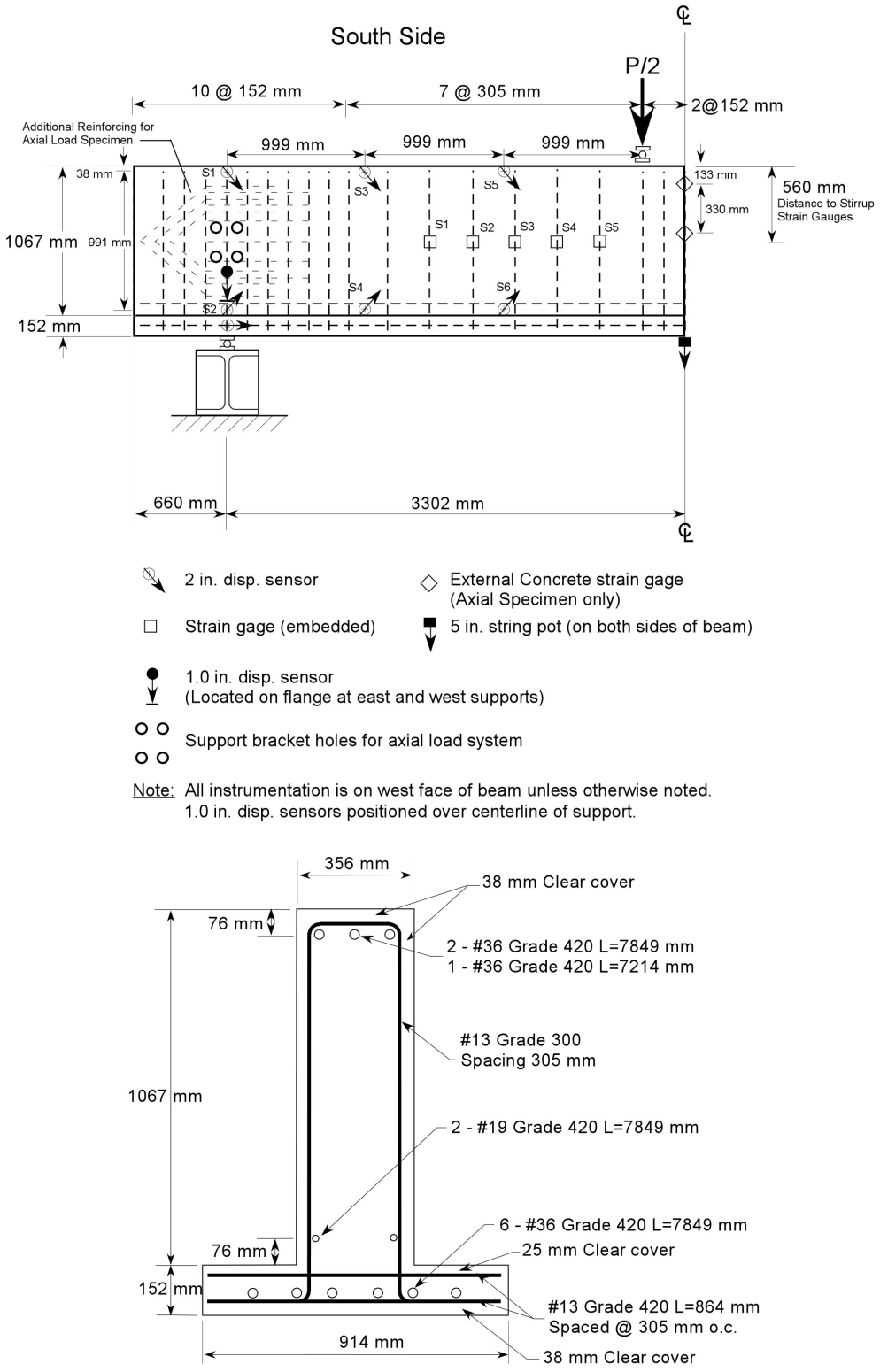

Fig. 2.1: Specimen reinforcing details and typical instrumentation schematic.

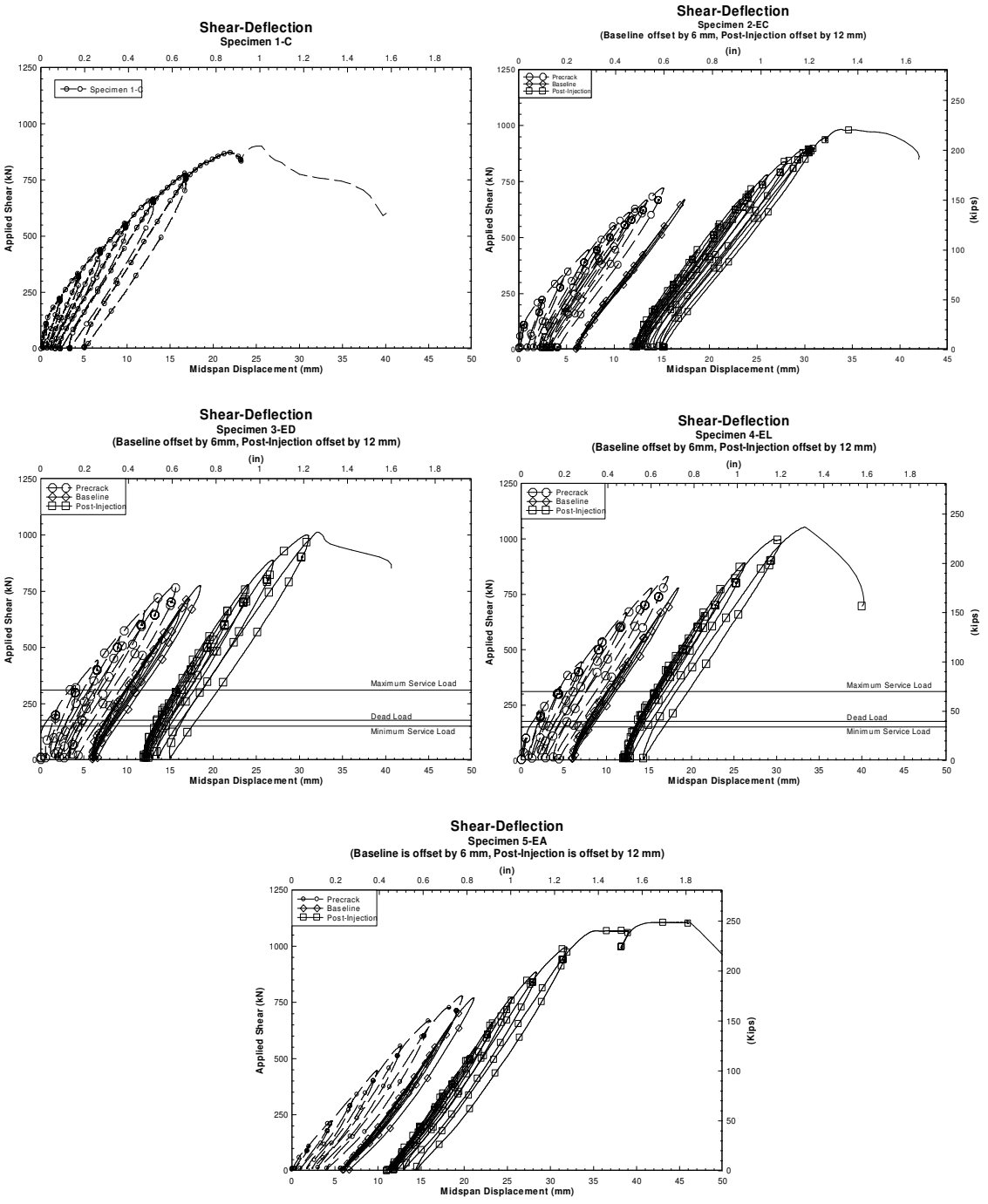

Fig. 2.2: Shear-midspan displacement response.

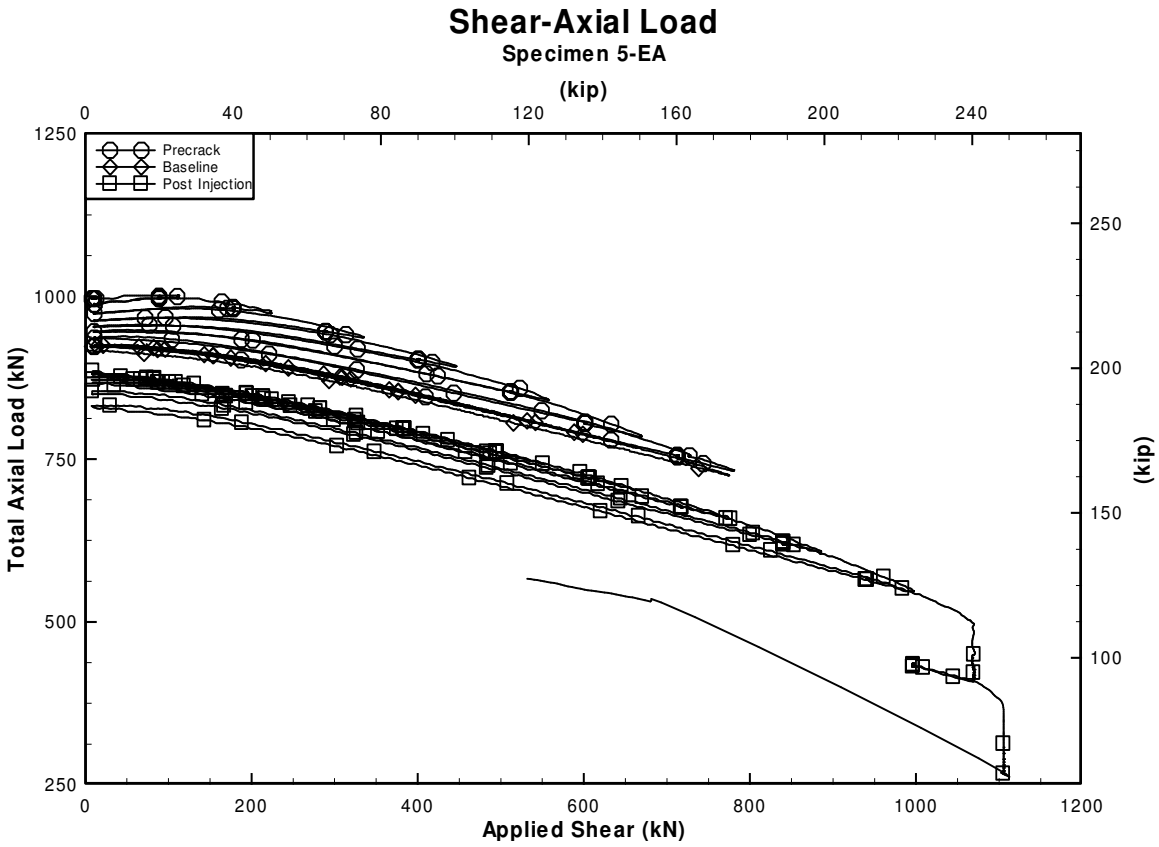

Fig. 2.3: Shear-axial load variability of specimen 5-EA.

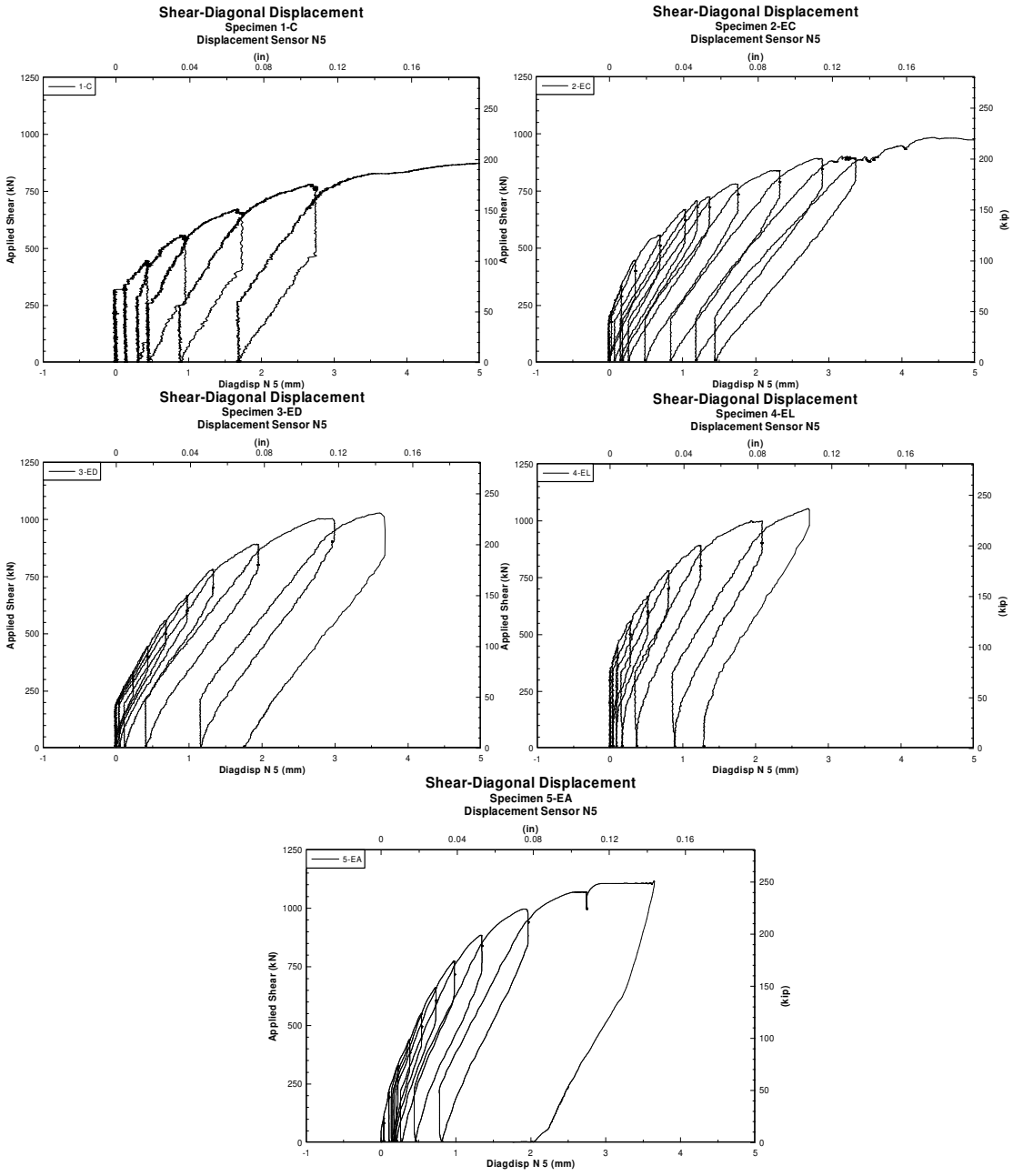

Fig. 2.4: Shear-diagonal displacement response. Values were recorded near centerline of specimens on north side.

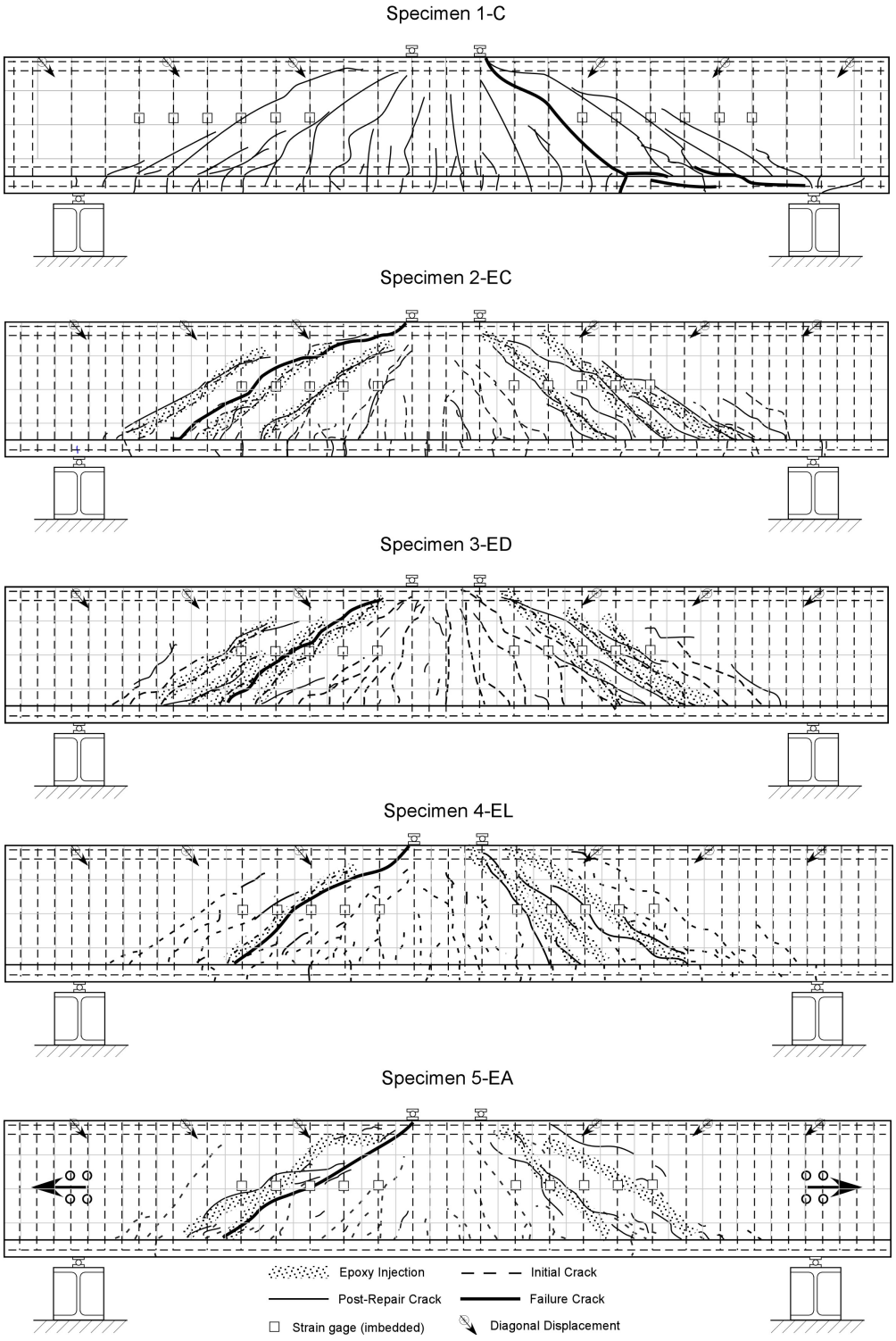

Fig. 2.5: Crack pattern locations on east face of specimens. Figure includes precracking, epoxy injected cracks, post-injection cracks, and final failure crack.

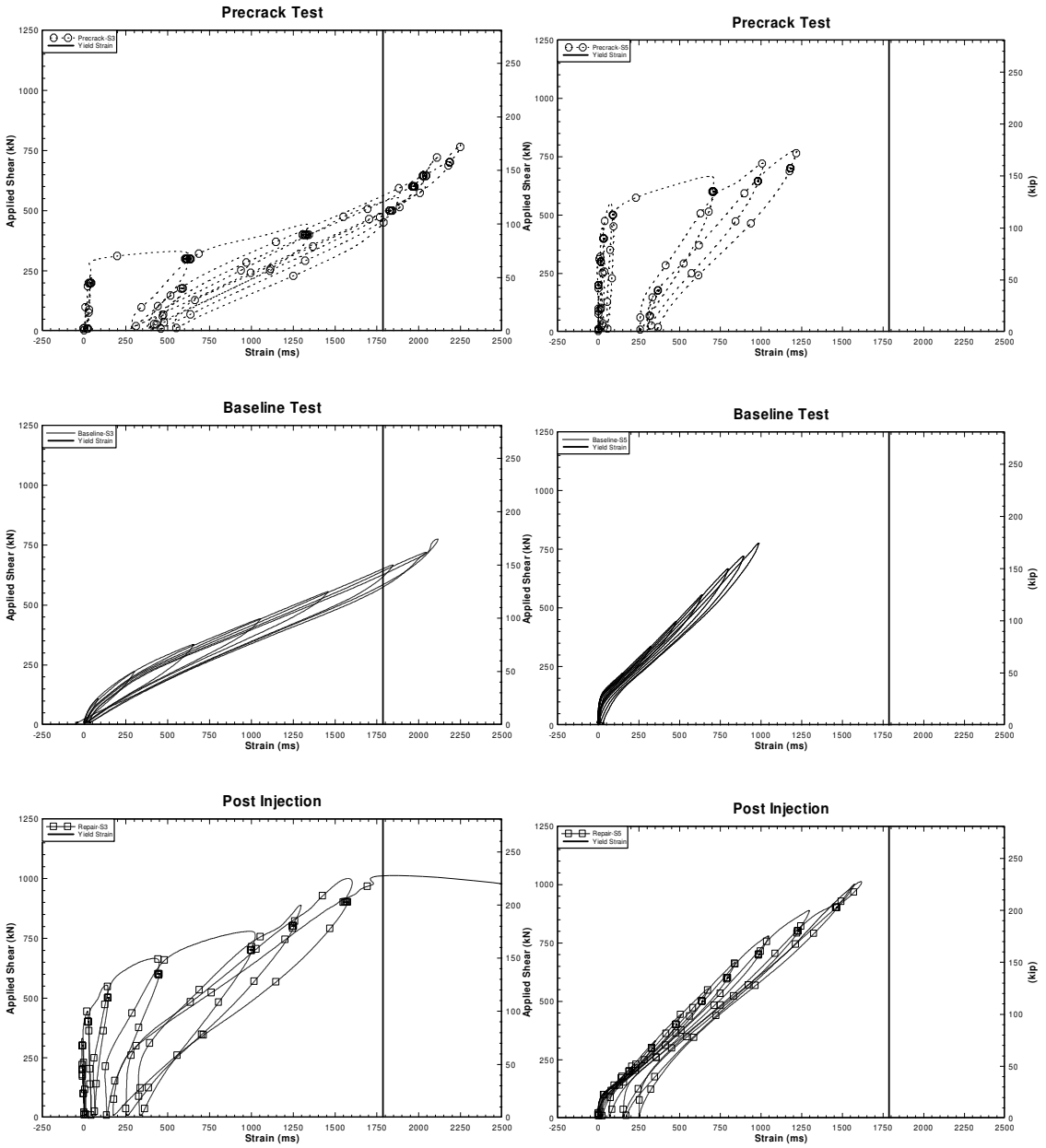

(a) Near Injected Crack (b) Near Un-injected Crack

Figure 2.6: Applied shear-stirrup strain behavior for specimen 3-ED. Strain gages located near (a) injected diagonal cracks and (b) un-injected diagonal cracks.

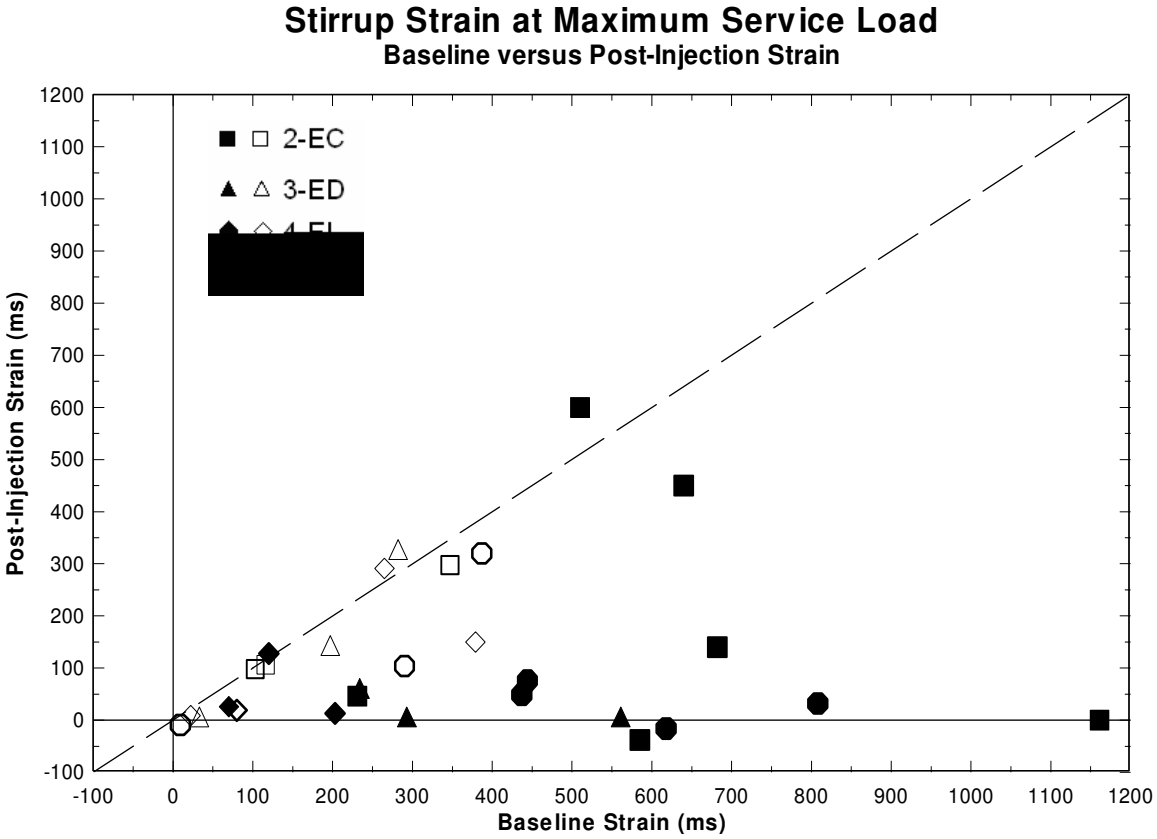

Fig. 2.7: Stirrup strains at maximum service level shear before and after injection.
Shear magnitude at 311 kN (70 kip)
Solid symbol: sensor located near injected diagonal crack
Hollow symbol: sensor located far from injected diagonal crack

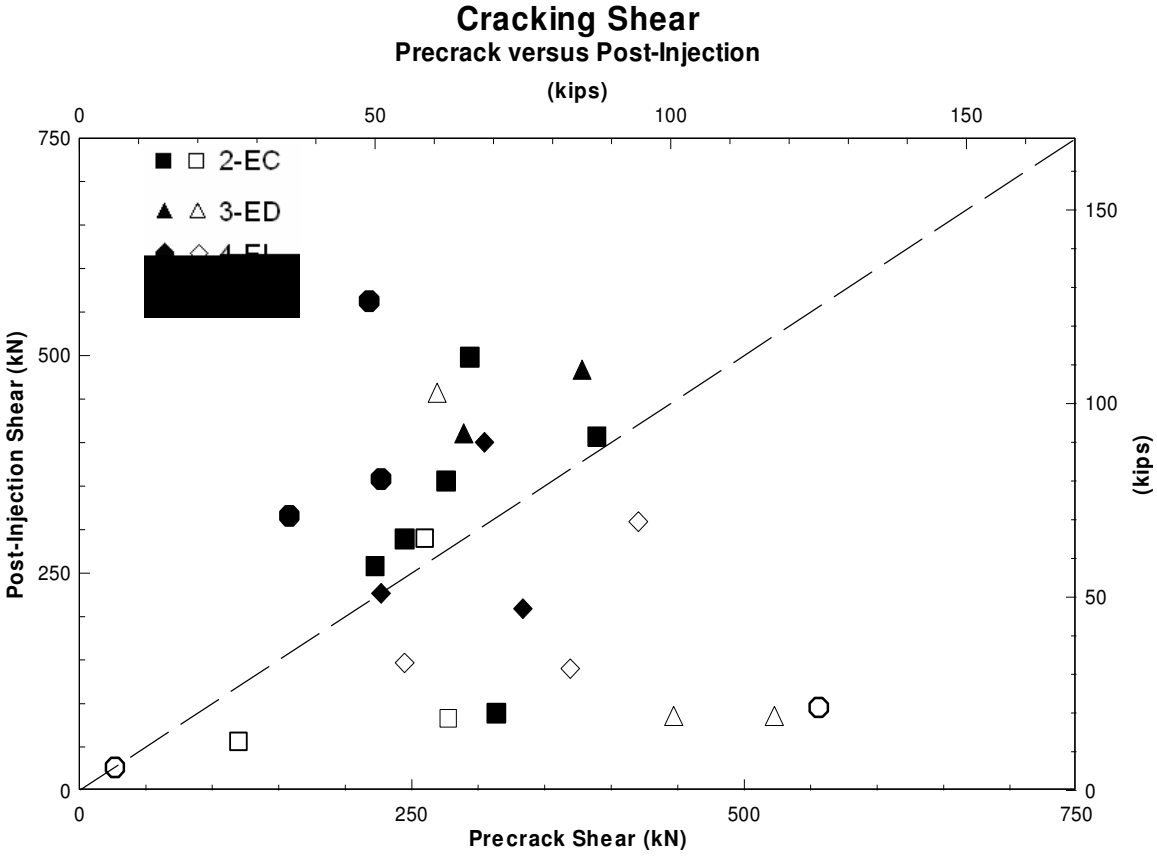

Fig. 2.8: Applied shear at diagonal cracking initiation before and after injection.
Solid symbol: sensor located near injected diagonal crack
Hollow symbol: sensor located far from injected diagonal crack

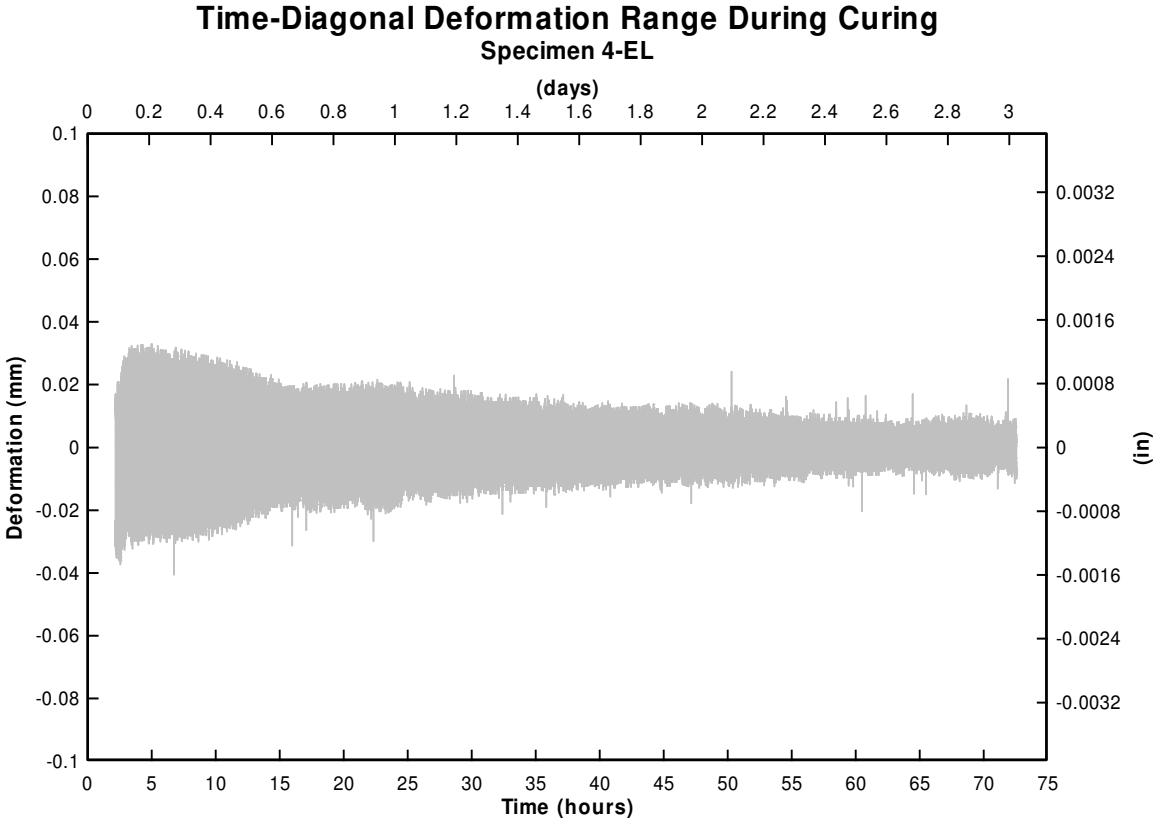

Fig. 2.9: Diagonal deformation range during curing of specimen 4-EL.

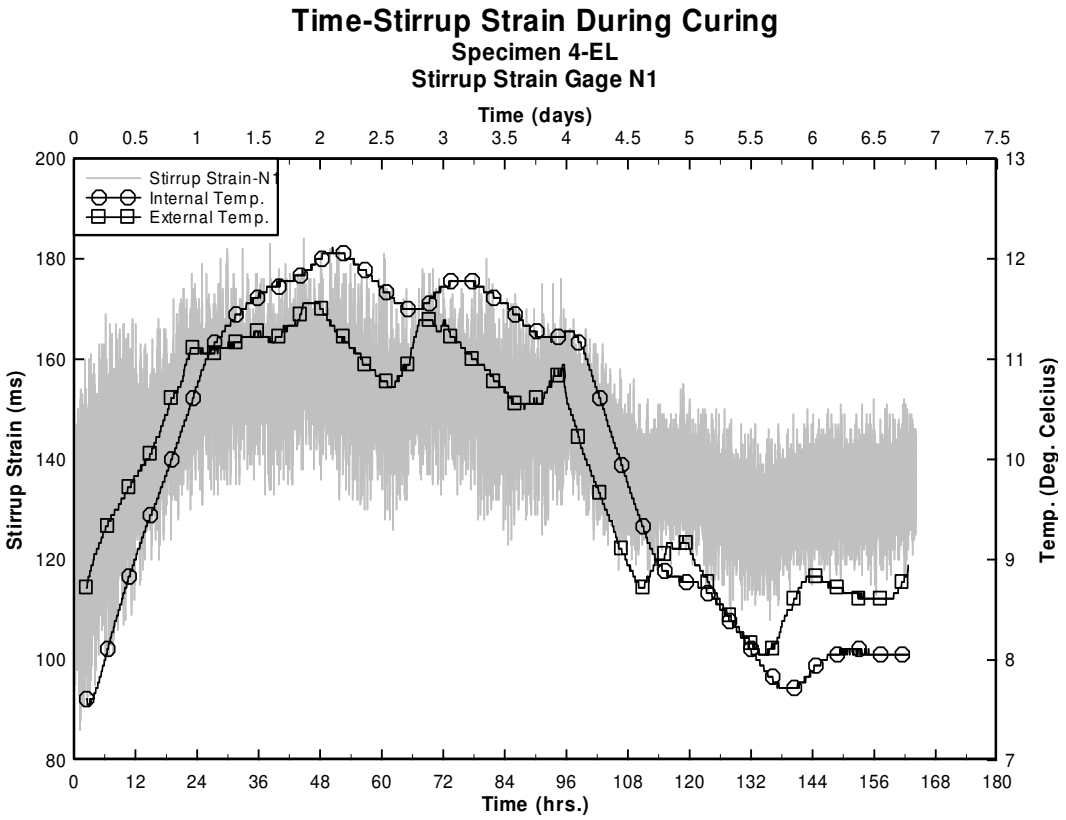

Fig 2.10: Stirrup strain during curing of specimen 4-EL

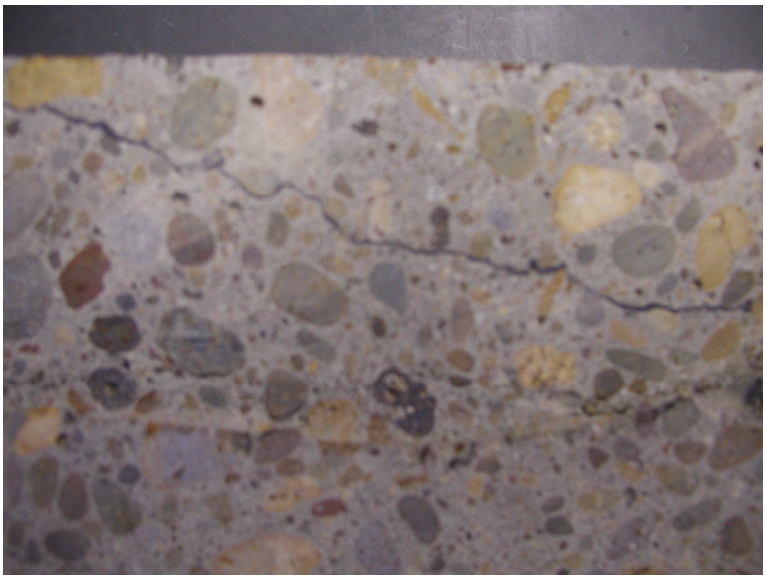

(A)

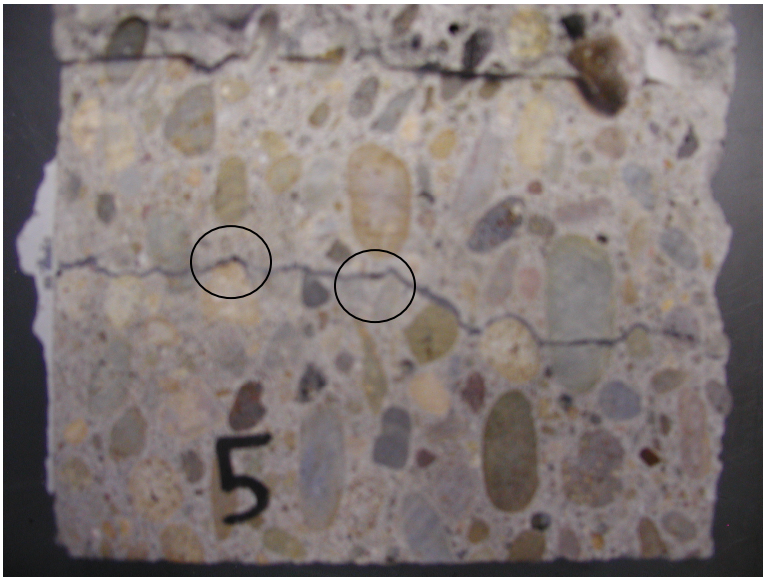

(B)

Fig. 2.11: Photographs of cores taken from specimens 3-ED and 4-EL.
(A) Core taken from specimen 3-ED.
(B) Core taken from specimen 5-EA with small voids.

Investigation of the Effects of Imposed Axial Tension on Diagonally Cracked Full-Scale CRC Deck-Girders

Matthew Smith, Daniel Howell, and Christopher Higgins

American Society of Civil Engineers

Journal of Bridge Engineering

1801 Alexander Bell Dr.

Reston, VA 20191

To be published

Introduction and Background

Large numbers of cast-in place reinforced concrete deck-girder (RCDG) bridges remain in the national inventory and are reaching the end of their originally intended design lives. Some states, like Oregon, principally constructed RCDG bridges during the 1950s and 1960s as the interstate highway system was expanded. In 2001, the Oregon Department of Transportation (ODOT) identified nearly 500 RCDG bridges as exhibiting varying degrees of diagonal-tension cracking in the girders and bent caps. Diagonal-tension cracks may be caused by overestimation of concrete contribution to shear resistance and poor reinforcement details, increasing service load magnitudes and volume, as well as temperature and shrinkage effects. Rating and evaluation of existing bridges has begun to move toward the AASHTO-LRFR approach, which states that temperature and shrinkage effects may be ignored when calculating load ratings for bridge components with well distributed reinforcement. However, the definition of well distributed reinforcement is not established, and it is unlikely that 1950's vintage bridge girders with straight-bar cutoffs in flexural tension regions and light shear reinforcement would be considered as meeting such a criteria. The treatment of axial tension effects from direct loading and indirectly from shrinkage and temperature effects on member shear-moment capacity is not well established. Research was undertaken on large-size realistically proportioned girders to investigate this interaction.

A significant amount of previous research has been conducted to characterize shrinkage and temperature strains in concrete. Committee 209R-92 of the American Concrete

Institute (1992) and CEB-FIPC (1990) provide methodologies for estimating shrinkage and temperature strain magnitudes. Significant uncertainty in predicting these effects remain as described by ACI Committee 209;

> "While these methods yield reasonably good results, a close correlation between the predicted deflections, cambers, prestress losses, etc. and the measurements from field structures should not be expected."

Furthermore, the report notes that many of the analysis methods presented are simplified and the use of supplemental test data would be needed to improve prediction and service performance. An experimental program by Bryant and Vadhanavikit (1987) studied the shrinkage and creep behavior of 100-400 mm (3.9-15.7 in.) plain concrete slabs and prisms. Specimens were cast and aged for over 5 years in carefully controlled environments and the shrinkage measurements collected were compared with ACI Committee 209 estimates. Bryant and Vadhanavikit suggested from their results that the ACI 209 predictions are un-conservative and may underestimate creep and shrinkage strains for large-scale specimens.

Like Bryant, others have studied large concrete specimens and the effects of differential temperature on crack propagation and concrete surface strains. Hughes and Mahmood (1988) investigated the effects of early thermal gradients in 1500 x 600 x 150 mm (59 x 24 x 6 in.) reinforced concrete slabs. They observed that the number and spacing of cracks were related to the temperature differential in addition to the amount, diameter, and depth of reinforcement.

The propagation of cracks plays an important role in the performance of concrete structures. Much of the nonlinear response of a concrete specimen is comprised of the cracking of concrete in tension. To better understand this behavior, many previous studies have investigated the stress-strain and cracking behavior of reinforced concrete specimens in uniaxial tension. Rizkalla and Hwang (1984) proposed a methodology for predicting crack spacing and width for reinforced concrete beams subjected to uniaxial tension. Specimens in the study were reinforced with longitudinal and transverse reinforcement and measured 305 x 254 mm (12 x 10 in.) in cross section and 762 mm (30 in.) long.

Li, *et al.* (2002) studied the behavior of 250 x 250 x 500 mm (9.8 x 9.8 x 19.7 in.) reinforced concrete specimens in uniaxial tension. They observed the stress-deformation responses and developed a relationship between the compressive and tensile strengths. Their findings concluded that tensile strengths tend to be smaller for larger aggregate sizes compared to estimates developed from small-sized aggregate concrete.

Limitations in the existing data include small specimen size, few specimens with realistic flexural and shear reinforcement details, and loading conditions. Methods to determine performance and capacity of conventionally reinforced concrete (CRC) specimens with shear-tension-flexural loading have not been produced or fully validated. An experimental program was conducted to characterize the behavior and the capacity of full-size CRC girders with 1950's vintage details under varying axial tension effects.

Research Significance

Many RCDG bridges with diagonal cracks remain in service today and the effects of temperature and shrinkage on member shear-moment capacity are not well established. Leading codes for design and rating of bridges neglect the effects of temperature and strain for well detailed bridge components, but 'well detailed' is not clearly defined. An experimental program was conducted using large-size realistically proportioned girders with straight-bar cutoffs and light shear reinforcement to study the role of externally applied axial tension on shear-moment capacity.

Experimental Program

Test Specimens

Seven laboratory specimens were constructed and tested to characterize the behavior and capacity of 1950's vintage CRC deck girders under combined transverse loading and axial tension. Previous work by Higgins *et al.* (2004, "SPR 350") identified standard details, materials, and member proportions used in 1950's vintage bridge construction. Specimens in this study used these proportions with an inverted-T configuration to place the deck in flexural tension. This arrangement is representative of negative moment in high-shear locations near continuous supports such as piers and bent caps. Each specimen had the same geometry measuring 1219 mm (48 in.) overall height, with a stem width of 356 mm (14 in.), and a deck flange 152 mm (6 in.) thick by 914 mm (36 in.) wide. Figure 3.1 illustrates the member proportions and reinforcing steel details. Longitudinal

reinforcing steel consisted of ASTM A615 Grade 420 #36 (Gr. 60, #11) bars and Grade 300 #13 (Gr. 40, #4) stirrups were used for transverse reinforcement. Tension tests were performed to determine the reinforcing steel properties which are summarized in Table 3.1. Two specimens identified as 2-CC and 6-AC, were fabricated with straight flexural bar cutoff details, as illustrated in Fig. 3.1. Transverse reinforcing steel in the failure region was placed 305 mm (12 in.) on-center. This spacing was reduced at the simple support locations and combined with additional reinforcement to prevent failure of the end sections under applied axial tension.

Concrete was provided by a local ready-mix supplier for all specimens. The concrete mix design was based on 1950's AASHO "Class A" concrete used in previous research at OSU (Higgins *et al.*, 2003). Specified compressive strength was 21 MPa (3000 psi), which is comparable to the specified design strength in the original 1950's bridges. Actual concrete compressive strengths were determined from 152 x 305 mm (6 x 12 in.) cylinders tested for 28 day and day-of-test strengths in accordance with ASTM C39M/C 39M-05 and ASTM C617-05. Day of test concrete cylinder strengths for each specimen are shown in Table 3.1 The aggregate composition for the mix was reported by the supplier as: 97% passing the 19 mm sieve (3/4 in.), 82% passing 16 mm (5/8 in.), 57% passing 12.5 mm (1/2 in.), 33% passing 9.5 mm (3/8 in.), 21% passing 8 mm (5/16 in.), 9.3% passing 6.3 mm (1/4 in.), 3.0% passing 4.75 mm (#4), 0.6% passing 2.36 mm (#8) and 0.3% passing the 0.075 mm (#200) sieve. The sand composition of the mix was also reported as: 99.7% passing the 6.3 mm sieve (1/4 in.), 96.8% passing 2.36 mm (#8),

59.4% passing 1.18 mm (#16), 44.9% passing 0.600 mm (#30), 17.9% passing 0.300 mm (#50), 3.7% passing 0.150 mm (#100) and 1.7% passing the 0.075 mm (#200) sieve. The coarse aggregate was from Willamette River bed deposits consisting of smooth rounded basaltic rock.

Instrumentation

Internal and external sensors were positioned on the specimens to record the local and global member responses. Strain gages were placed on stirrups located within the critical section near midspan. Additional strain gages were mounted to the flexural reinforcement at midspan in the flexural tension region and also on the concrete surface. Displacement transducers were placed within three regions on each end the beam to measure diagonal deformations and at the centerline of supports to measure overall specimen elongation. Support settlements were measured with additional displacement transducers located at the centerline of supports perpendicular to the flange. Midspan displacements were measured with string potentiometers. The actual specimen centerline displacement represented in subsequent figures was calculated by removing the support deformations from the overall deformation during each test. The typical instrumentation plan is illustrated in Fig. 3.1.

Testing Methodology

A simply-supported loading configuration was used with a span length of 6604 mm (260 in.) between centerline of bearings. Axial load was applied by two 890 kN (200 kip) hydraulic cylinders, mounted on each side of the specimen stem by steel brackets mounted with four high-strength 32 mm (1.25 in.) diameter A193-B7 threaded rods. The supporting brackets were positioned at the centerlines of support on the geometric centroid of the gross uncracked section. 152 x 152 x 10 mm (6 x 6x 3/8 in.) HSS tubes transferred the axial load to a bracket located at the opposite end of the member. The axial loading setup is illustrated in Fig. 3.2. Axial tension was typically applied in 222 kN (50 kip) increments and the force in each tube was measured directly with 890 kN (200 kip) capacity load cells. At each axial load increment, cracks were marked on the specimen and measured. The hydraulic fluid pressure was stabilized during transverse loading by a nitrogen gas accumulator. In all axially loaded specimens except 6-AV, the tension was fully applied before the transverse load. For specimen 6-AV, the axial load was applied in proportion to the transverse load as described subsequently. The transverse force was applied with a hydraulic actuator operating at a constant rate of 8.9 kN/sec (2.0 kips/sec) and was measured by a 2224 kN (500 kip) capacity load-cell. A spreader beam distributed the applied actuator force to 102 mm (4 in.) wide plates spaced 610 mm (24 in.) symmetrically about midspan in a four-point loading configuration. Load was applied at incrementally increasing peaks followed by unloading. Load

magnitudes increased each cycle by an amount of 222 kN (50 kips). At each load peak, the load was reduced by 10% and then held constant to minimize creep effects while cracks were marked and measured.

Specimen Variables

The experimental program incorporated a number of parameters to study the effects of variable axial tension, flexural bar cut-offs, and epoxy injection of diagonal cracks. Specimen 1-C contained full-length hooked flexural bars while specimen 2-CC contained cutoff straight flexural bars representative of mid-twentieth century design practice that allowed for flexural cutoffs in flexural tension zones. Specimen 6-AC also contained cutoff flexural bars. Specimen 1-C and 2-CC were control specimens not subjected to axial load. The remainder of the specimens were subjected to 890 kN (200 kip) of axial load with the exception of specimen 4-A3 which had 1334 kN (300 kip) applied axial load. The axial force magnitudes used in the study were chosen to reflect the longitudinal tension forces developed from restraint of bridge girder movements in the field from drying shrinkage and temperature changes. Previous work by Higgins et al. (2004, "SPR 341") predicted the drying shrinkage strains of RCDG bridge components using CEB-FIP methods. The member proportions and concrete material properties and curing conditions of the bridge members were incorporated in the method. Relative humidity was assumed to be 40% (Oregon Climate Service), moist curing time was taken as 14 days, and age concrete was assumed to be greater than 365 days. Shrinkage strains for the RCDG girders were estimated to be approximately 0.0002. Typical annual thermal contraction

strains were assumed to result from a 14.5 ^{o}C (26 ^{o}F) temperature change with a construction reference temperature of 12.8 ^{o}C (55 ^{o}F). Elastic finite element analysis was performed on a full model of a 3-span continuous bridge with 15.2 m (50 ft) spans. Linear spring elements were used to represent the abutment-girder friction assuming a coefficient of static friction of 0.5 to approximate a concrete-steel interface. Results of the finite element analysis yielded shrinkage and thermal longitudinal stresses of approximately 1310 and 930 MPa (190 and 135 psi), respectively for girders near midspan. These stresses correlate to axial longitudinal forces of approximately 680 and 483 kN (153 and 109 kip) for the laboratory girder cross-sectional area. An applied axial force magnitude of 890 kN (200 kip) was selected to represent amplified shrinkage stresses and the 1334 kN (300 kip) force the combined influence of shrinkage and thermal contraction.

Specimen 5-AE was used to study the effects of epoxy injection combined with axial tension on behavior and capacity. The procedures used for inducing initial diagonal cracking and epoxy injection of the specimen are described in detail in Chapter 2 of this report. Unlike the other axial load specimens, specimen 5-AE did not have an accumulator to maintain the hydraulic pressure as the transverse loading was applied. This was done to examine the variability of axial load in response to applied transverse load. The axial load reduced as the transverse load was applied, decreasing over time as the transverse force increased as shown in Fig. 2.3. Similarly, specimen 7-AV had variable axial load that was applied in proportion to the transverse load. This was

performed in order to investigate possible path-dependency of the axially loaded specimens. The transverse and axial loads were applied simultaneously at a ratio of 7:1 to achieve the observed strength of specimen 7-AV.

Experimental Results and Discussion

The performance of each of the specimens was evaluated through the applied shear-deformation responses, flexural and shear reinforcement strains, and crack deformations. Global and local member responses were compared between specimens to assess the effect of axial load on internal stress distribution and deformations.

In a previous study, a computer program called Response 2000 (R2K) (Bentz, 2000), which utilizes Modified Compression Field Theory (MCFT), was used to predict shear capacity for a series of 31 otherwise similar full-size CRC specimens. The program predicted capacity to within 0.98 of actual with a coefficient of variation under 8% (Higgins *et al.*, "Spring 350," 2004) for specimens not subjected to axial loads. R2K was used to estimate the inherent capacities of the specimens with and without applied axial load as well as the strength of the control specimens. ACI 318 (ACI, 2004) and AASHTO-LRFD (AASHTO, 2004) equations for estimating shear capacity were also included in the prediction. From chapter 11 of ACI 318, shear strength is computed for members subjected to significant axial tension as:

$$V_n = V_c + V_s \tag{1}$$

$$V_c = 2(1 + \frac{N_u}{500A_g})\sqrt{f'_c}b_w d \tag{2}$$

$$V_s = \frac{A_v f_{yt} d}{s} \tag{3}$$

Chapter 5 of the AASHTO LRFD Bridge Design Specification computes the shear capacity for non prestressed members as:

$$V_n = V_c + V_s \tag{4}$$

$$V_c = 0.0316\beta\sqrt{f'_c}b_v d_v \tag{5}$$

$$V_s = \frac{A_v f_y d_v (\cot\theta + \cot\alpha)\sin\alpha}{s} \tag{6}$$

Where β and θ are computed based on the shear stress normalized with respect to concrete compressive strength ε_x, which is computed as:

$$\varepsilon_x = \frac{(\frac{M_u}{d_v} + 0.5N_u + 0.5(V_u - V_p)\cot\theta - A_{ps}f_{po})}{2(E_s A_s + E_p A_{ps})} \tag{7}$$

Bentz integrated the AASHTO-MCFT equations and tables into a spreadsheet that directly computes the shear-moment interaction (2000). The predicted shear strengths for all methods are summarized in Table 3.2. For each prediction, the axial load at the moment of failure was used in the analyses. For the cutoff details of specimens 2-CC and 6-AC, reduced amounts of flexural bar area were obtained by multiplying the full cross-sectional area of flexural bars by a ratio of actual embedded length to the AASHTO-

LRFD development length of the flexural bars. The actual embedded length was the distance from the end of the bar to the critical section of the beam taken at d_v (the distance between the flexural tension and compression resultants) from the edge of the loading plate near midspan.

All three methods tended to underestimate the shear capacity of the specimens. R2K predicted shear capacities closest to the actual observed values while ACI was the furthest away. The averages and coefficients of variation (COV) for the capacity predictions are shown in Table 3.2 for the axially loaded specimens excluding the epoxy injected specimen. The smallest COV was 2% for the AASTHO-MCFT predictions which were approximately 11% under the actual capacities.

The largest disparity between actual and estimated capacity was for specimen 5-AE. This was more likely a function of the loading protocol and epoxy injection process than that of epoxy-axial tension interaction. Specimen 5-AE was epoxy injected with a constant axial force of 645 kN (145 kip) after formation of diagonal cracks. At failure, the axial tension in specimen 5-AE was only 267 kN (60 kip) equating to a net release of compression into the specimen of 378 kN (85 kip), thereby effectively post-tensioning the girder during failure testing and increasing the capacity. For non-axially loaded specimens, epoxy injection of diagonal cracks was observed to only slightly increase capacity as summarized in Chapter 2.

R2K predicts lower shear capacities for specimens with axial tension or flexural cutoff details, and when combined, the capacity is reduced even further. From the experimental results, it was observed that capacity was generally lower for axially loaded or cutoff specimens, but was not significantly lower when both conditions applied. R2K over-predicted the capacity of specimen 6-AC by 16%. This may be a result of the failure mechanism which was shear-compression for all seven specimens. Imposed axial tension may delay such a failure by reducing the compressive strain of the concrete compressive zone thereby allowing the flexural steel to reach larger tension strains. Combined with flexural cutoffs which also increase flexural reinforcement tension shown in subsequent figures, the failure mode nearly became shear-tension for specimen 6-AC. This interaction is likely the cause of the increased capacity of specimen 6-AC.

Fig. 3.3 displays the predicted shear-axial load capacity of the test specimens with the experimental values. Also displayed are the R2K, ACI, and AASHTO estimates for a typical girder without cutoffs and idealized material properties of f'_c = 29.9 MPa (4330 psi), f_{yl} = 483 MPa (70.1 ksi), and f_{yt} = 353 MPa (51.2 ksi) with variable axial load ranging from 0-2224 kN (0-500 kip). It is observed from the figure that R2K initially over-estimates capacity for low axial values which is consistent with experimental results from Higgins *et al.* ("Spring 350," 2004) With increasing axial tension, R2K becomes more conservative. AASHTO tends to under-estimate capacity for all axial tension

specimens, while ACI significantly under-estimated capacity. Additional data is needed to quantify statistical uncertainties for moment and shear combined with axial tension above that reported in this study.

Overall shear-midspan deflection responses are shown in Fig. 3.4. The presence of axial tension softened specimen response, producing additional residual deformations at each load step as compared to control specimen 1-C. Specimen 4-A3 had reduced stiffness compared to specimen 3-A2 and exhibited larger deflections at similar transverse load magnitudes. The reduction of flexural steel in the flexural tension region also softened the behavior as seen by comparing specimen 2-CC with 1-C. When axial load was included with cutoff detailing, as with specimen 6-AC, the stiffness reduction increased, but the overall capacity remained similar. The variable loading of specimen 7-AV initially altered the shape of the load-deflection response, but did not significantly change total deformation after each load step compared to specimen 3-A2. With increasing load magnitudes, the responses of specimens 7-AV and 3-A2 became more similar.

Similar to the midspan displacement, the diagonal deformation response to shear was influenced by axial load and flexural cut-off details. Fig. 3.5 shows representative responses for each specimen. The presence of either axial load or flexural cutoffs resulted in larger diagonal deformations, but when axial load was combined with reduced flexural steel, the effects where amplified. Specimen 4-A3 was softer than specimen 3-A2, and specimen 6-AC was softer than either specimens 2-CC or 3-A2. The post-injection

response of specimen 5-AE was stiffer and exhibited decreased residual deformations than either specimen 1-C or 3-A2, as well as the baseline and precrack tests discussed in Chapter 1. Specimen 7-AV was initially stiffer than specimen 3-A2, because diagonal cracking was coupled with axial tension effects rather than first producing tension cracking and then diagonal cracking. At higher load magnitudes specimens 3-A2 and 7-AV became more similar.

The load required to induce diagonal cracking after application of axial tension was determined from the diagonal displacement measurements along the length of the specimens. Diagonal cracking load was identified as the shear force that induced an abrupt change in the diagonal deformation for the first time. Table 3.2 shows the applied shear force at diagonal cracking. Control specimen, 1-C, exhibited a higher cracking load than the other specimens except 5-AE after injection. The diagonal cracking shears of the axially loaded and flexural cutoff specimens were significantly lower than specimen 1-C. Specimen 5-AE had a much higher cracking load on the south end only. The north end of specimen 5-AE was considerably lower. This discrepancy is a result of the location of epoxy injected diagonal cracks compared to the diagonal displacement sensors. The north section of specimen 5-AE had more numerous small cracks that could not be injected, which produced diagonal deformations upon reloading as compared to the south section which had the diagonal cracks bonded by the epoxy. Both sides of specimen 1-C cracked at approximately the same load, while the axial specimens were more variable. Generally, one side cracked diagonally at a slightly lower shear than the other side.

The growth of the diagonal and vertical cracks were recorded as shown in Fig. 3.6. As axial tension was applied, vertically orientated cracks were observed to form initially over stirrup locations. As transverse load was applied, the vertical cracks closed to hairline or below above mid-height of the stem and diagonal cracks began to form in a manner and shape similar to the control specimens. The diagonal crack angles were only slightly steeper for specimens 6-AC and 7-AV then for the specimens 1-C and 2-CC. Failure modes for all specimens were shear-compression. Wide flexural cracks formed at the location of the cut flexural bars for specimens 2-CC and 6-AC, and propagated diagonally toward the loading plate. The other specimens had similar cracks at failure, but their originating points were not apparent until failure occurred.

Unlike the diagonal and midspan displacements, the steel strains were more variable depending on the sensor location relative to the crack locations for different specimens. Generally, the stirrup strain gages did not measure compression strains for the control specimens. However, several of the stirrup strain gages for the axially loaded specimens were observed to measure compressive strains during the initial axial tensioning while other stirrup strain gages measured tension. The tension and compression strains induced by the axial load were typically small, below 100 $\mu\varepsilon$. As transverse load was applied, all stirrup strains became tensile and increased substantially upon formation of diagonal cracking.

The effects of the axial tension on the flexural reinforcement strain were small but distinct as seen in Figs. 3.7 and 3.8. Fig. 3.7 shows the transverse shear-midspan flexural reinforcing strain responses of each specimen, while Fig. 3.8 displays the axial tension-flexural rebar strain response. The transverse loading is not shown in Fig. 3.8 but is nonetheless evident by the sharp increases of strain with little change in axial load. The application of axial tension in Fig. 3.7 can be seen at the very beginning by the tensile strain movement for each specimen without increase in applied shear. In Fig. 3.7, Specimen 3-A2 and 4-A3 have similar response shapes and behaviors with the exception that specimen 4-A3 has higher strain at each shear magnitude. The difference amounts to approximately 300 $\mu\varepsilon$, which gradually increases with increasing shear magnitude. The stiffness of specimen 3-A2 is slightly greater than 4-A3. The precrack response (loading history before applying a peak applied cracking load) and post-injection responses are shown for specimen 5-AE. The axial tension magnitude for the pre-injection test was initially 1223 kN (275 kip), which was then reduced to approximately 880 kN (200 kip). This accounts for the lack of new cracking and linear response during the precrack transverse loading of specimen 5-AE. The post-injection response of specimen 5-AE has the highest slope of all the specimens. The response is almost entirely linear showing few signs of additional cracking that affected the flexural strain. The addition of flexural cutoffs softened the response of specimen 6-AC compared to specimen 3-A2. At early load peaks, the difference was small between the specimens, but at larger magnitudes near the end of the tests, strain differences became significant. Specimen 7-AV had axial and transverse load applied simultaneously as the loading was applied. Upon unloading

after each peak, the transverse load was reduced first, followed by the axial load. The increasing flexural demand on the steel as the specimen cracks is more apparent for specimen 7-AV than for the other specimens of similar axial load levels. The steel strain release is quite noticeable at zero transverse load which occurred as the axial load was removed. Overall, the flexural strains for specimen 7-AV tended to be higher than for specimen 3-A2.

The specimen elongation measured by the displacement transducers was used to determine the overall specimen strains shown in Fig. 3.9. From this, vertical tension cracking loads can be observed as the axial tension magnitude when the specimen elongation initially changes. Specimens 3-A2, 4-A3, and 6-AC have similar axial load-specimen strain responses with comparable vertical cracking tension loads. Specimen 7-AV is significantly different because of the combination of applied axial tension and transverse load. The axial tension has a significant effect on global specimen strain. A lower vertical cracking load for specimen 7-AV should be expected due to the interaction of shear and tension stresses in the web. The vertical cracking load for specimen 7-AV is approximately five times lower than for the other axial specimens.

Concrete strains were also directly measured at midspan near the top of the specimens (Fig. 3.1). Unlike the steel strain which varied significantly with axial tension, the concrete strain was nearly independent. The major influence on strain magnitude was the applied moment. Fig 3.10 displays the concrete compressive strains for specimens 5-AE

and 7-AV which both had variable axial loads throughout testing. Unlike the steel strains shown in Fig. 3.9, there are no dramatic increases or decreases in concrete strain resulting from applied axial tension. This indicates that the axial tension is carried almost exclusively through the reinforcing steel.

Conclusions

Seven CRC deck girders built to reflect the design and construction standards of 1950's vintage bridges were tested to study the effects of externally applied axial tension on member shear-moment capacity. Specimens were loaded to failure with varying degrees of axial tension applied in combination with transverse load. Factors included constant and variable axial tension as well as flexural cutoff detailing and epoxy injection. Based on the experimental observations and results, the following conclusions are presented:

- Superimposed axial tension reduced member shear-flexure capacity and reduced overall member stiffness.
- Initially applied axial tension reduced the transverse force required to initiate diagonal cracking.
- Axial load applied simultaneously with transverse load further reduced the transverse force required to initiate diagonal cracking.
- Reinforcing steel terminated in the flexural tension region combined with axial tension did not significantly reduce shear-flexure capacity beyond that of axial tension alone, for the shear-compression failure modes observed. Member capacity may be further reduced when shear-tension failures occur.

- The combined effects of flexural cutoffs and axial tension reduced global member stiffness beyond that of axial tension alone.
- R2K overestimated shear-flexure capacity for specimens with axial tension force of 890 kN (200 kip) and underestimated capacity for the specimen with tension force of 1334 kN (300 kip).
- AASTHO-LRFD and ACI 318-05 underestimated specimen shear capacity for all axial tension forces considered in this study.

REFERENCES

AASHTO LRFR, American Association of State Highway and Transportation Officials, "Manual for Condition Evaluation and Load and Resistance Factor Rating (LRFR) of Highway Bridges," Washington, DC., 2003

AASHTO LRFD, American Association of State Highway and Transportation Officials, "Load Rating and Factored Design (LRFD) Bridge Design Specifications," Washington, DC., 2004

ACI Committee 209, "Prediction of Creep, Shrinkage, and Temperature Effects in Concrete Structures," (ACI 209-R92), American Concrete Institute, Detroit, 1992, 47 pp.

ACI 318-05, "Building Code Requirements for Structural Concrete," American Concrete Institute, Farmington Hills, Michigan

Bentz, E., Repsonse 2000, University of Toronto, <http://www.ecf.utoronto.ca/~bentz/r2k.htm>.

Bentz, E., AASHTO Shear Calculator, University of Toronto

Bryant, A. H., and Vadhanavikkit, C., "Creep, Shrinkage-size, and Age at Loading Effects," American Concrete Institute Materials Journal, V. 84, No. 2, Mar.-Apr. 1987, pp. 117-123

Comite' Euro-International du Be'ton, CEB-FIP Model Code 1990, Thomas Telford Services Ltd. London, 1993

Higgins, C., Miller, T. H., Yim, S. C., Potisuk, T., and Robelo, M. J., "Research Project SPR 341: Remaining Life of Reinforced Concrete Beams with Diagonal-Tension Cracks," Oregon Department of Transportation, Salem, OR, April 2004, 110 pp.

Higgins, C., Miller, T. H., Rosowsky, D. V., Yim, S. C., Potisuk, T., Daniels, T. K., Nicholas, B. S., Robelo, M. J., Lee, A-Y., and Forrest, R. W., "Research Project SPR 350 SR 500-91: Assessment Methodology for Diagonally Cracked Reinforced Concrete Deck Girders," Oregon Department of Transportation, Salem, OR, Oct. 2004, 328 pp.

Hughes, B. P., and Mahmood, A. T., "Laboratory Investigation of Early Thermal Cracking of Concrete," American Concrete Institute Materials Journal, V. 85, No. 3, May-Jun 1988, pp. 164-171

Li, Q., Duan, and Y., Wang, G., "Behaviour of Large Concrete Specimens in Uniaxial Tension," *Magazine of Concrete Research*, V. 54, No. 5, Oct. 2002, pp. 385-391

Rizkalla, S. H., Hwang, L. S., "Crack Prediction for Members in Uniaxial Tension," *Journal of the American Concrete Institute*, V. 81, No. 6, Nov.-Dec. 1984, pp. 572-579

Table 3.1: Concrete and steel properties. Values are for day-of-test unless otherwise indicated.

Specimen	Concrete		Reinforcing Steel			
			#13-Grade 300		#36-Grade 420	
	f'c @ Failure (MPa)	Tensile @ Initial Loading (MPa)	Fy (MPa)	Fu (MPa)	Fy (MPa)	Fu (MPa)
1-C	28.5	3.2 @ 28-day	350	544	477	712
2-CC	33.4	2.7 @ 28-day			488	663
3-A2	23.4	2.3	357	570	477	702
4-A3	22.9	2.3			463	693
5-AE	35.4	2.8			492	741
6-AC	31.3	2.5			480	723
7-AV	29.4	2.4			478	722

Specimen	V_{exp} (kN)	V_{DL} (kN)	Vapp (kN)	Axial at Failure (kN)	V_{R2K} No Axial (kN)	V_{R2K} W/ Axial (kN)	V_{ACI} (kN)	V_{AASHTO} (kN)	V_{app}/V_{R2K}	V_{app}/V_{ACI}	V_{app}/V_{AASHTO}	Diagonal Cracking Shear (kN)
1-C	902	17	919	0*	950	-	703	810	0.97	1.31	1.13	322
2-CC	811	17	828	0*	828	-	733	805	1.00	1.13	1.03	219
3-A2	780	19	799	836	919	832	523	743	0.96	1.53	1.08	142
4-A3	783	12	795	1252	911	748	445	712	1.06	1.79	1.12	56
5-AE +	1112	18	1130	267	980	943	692	836	1.20	1.63	1.35	525
6-AC	806	13	819	791	823	704	560	721	1.16	1.46	1.14	153
7-AV	849	19	868	988	959	822	513	774	1.06	1.69	1.12	104
								Mean:	1.06	1.62	1.11	
								COV:	0.08	0.09	0.02	

Table 3.2: Specimen experimental summary.
* No axial loads were applied to specimens 1-C and 2-CC
+ Epoxy injection was not accounted for in the capacity estimate.

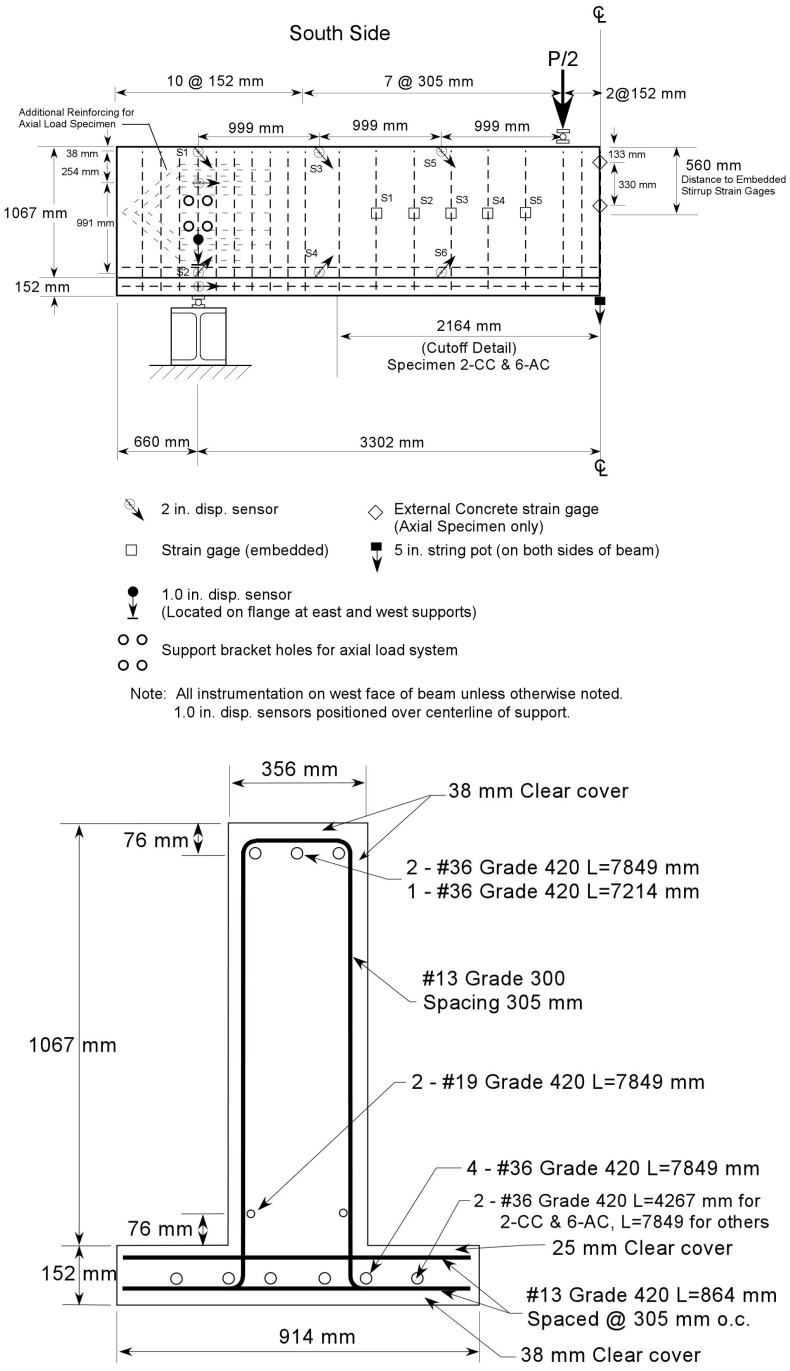

Fig. 3.1: Specimen reinforcing details and typical instrumentation placement.

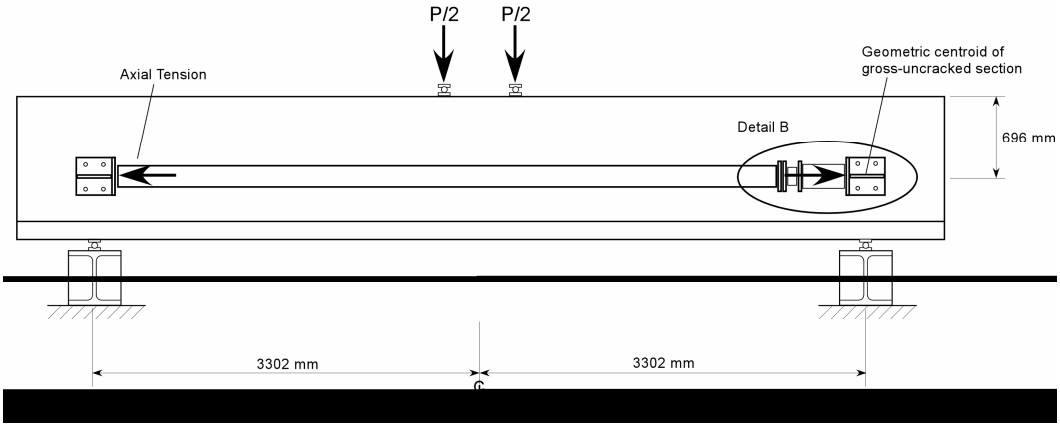

(A)

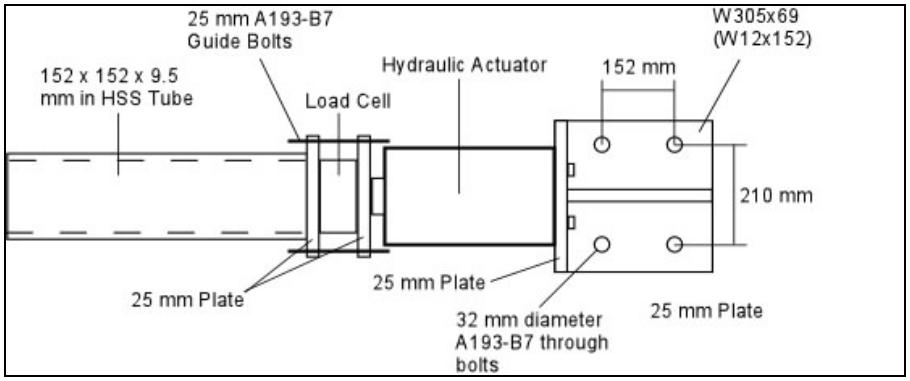

(B)

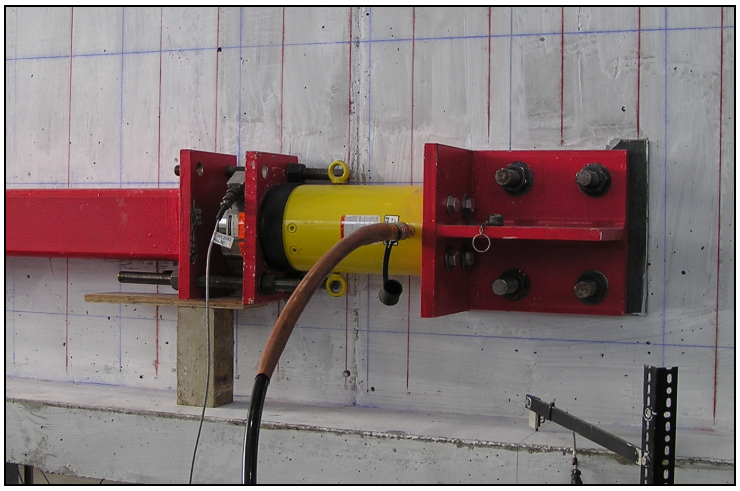

(C)

Fig. 3.2: Axial loading apparatus setup. (A) Specimen loading configuration (B) Detail B (C) Axial tension system photograph

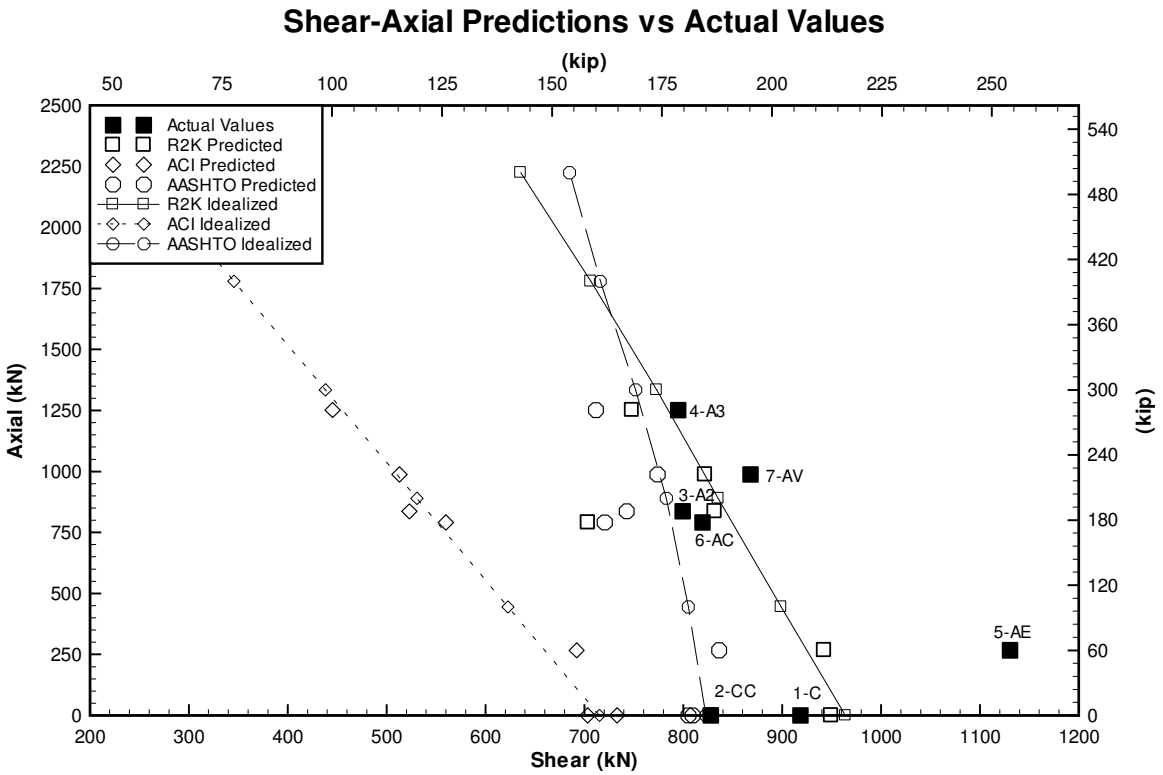

Fig. 3.3: Shear-axial load predictions compared to actual observed results.

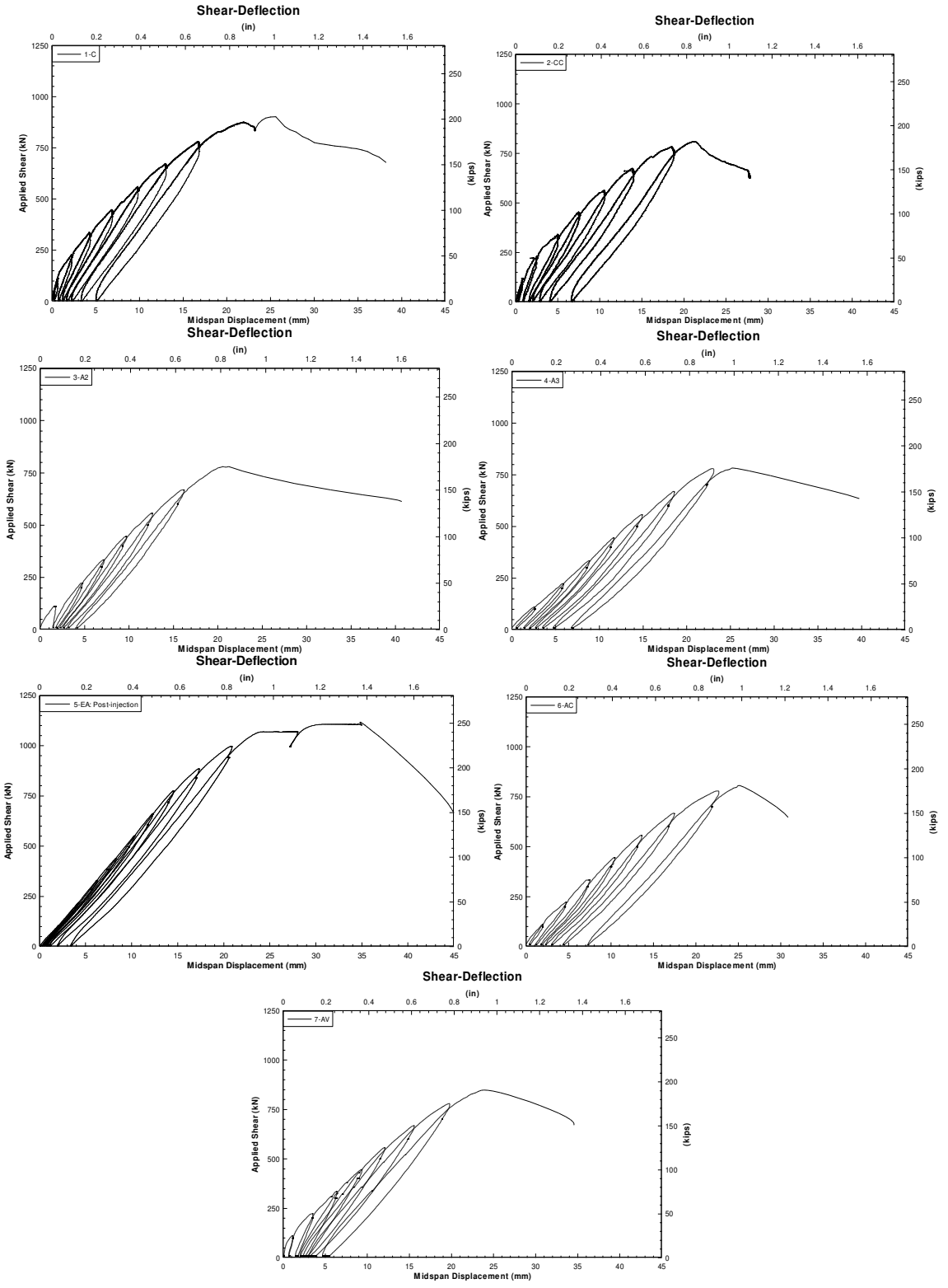

Fig. 3.4: Midspan shear-displacement response.

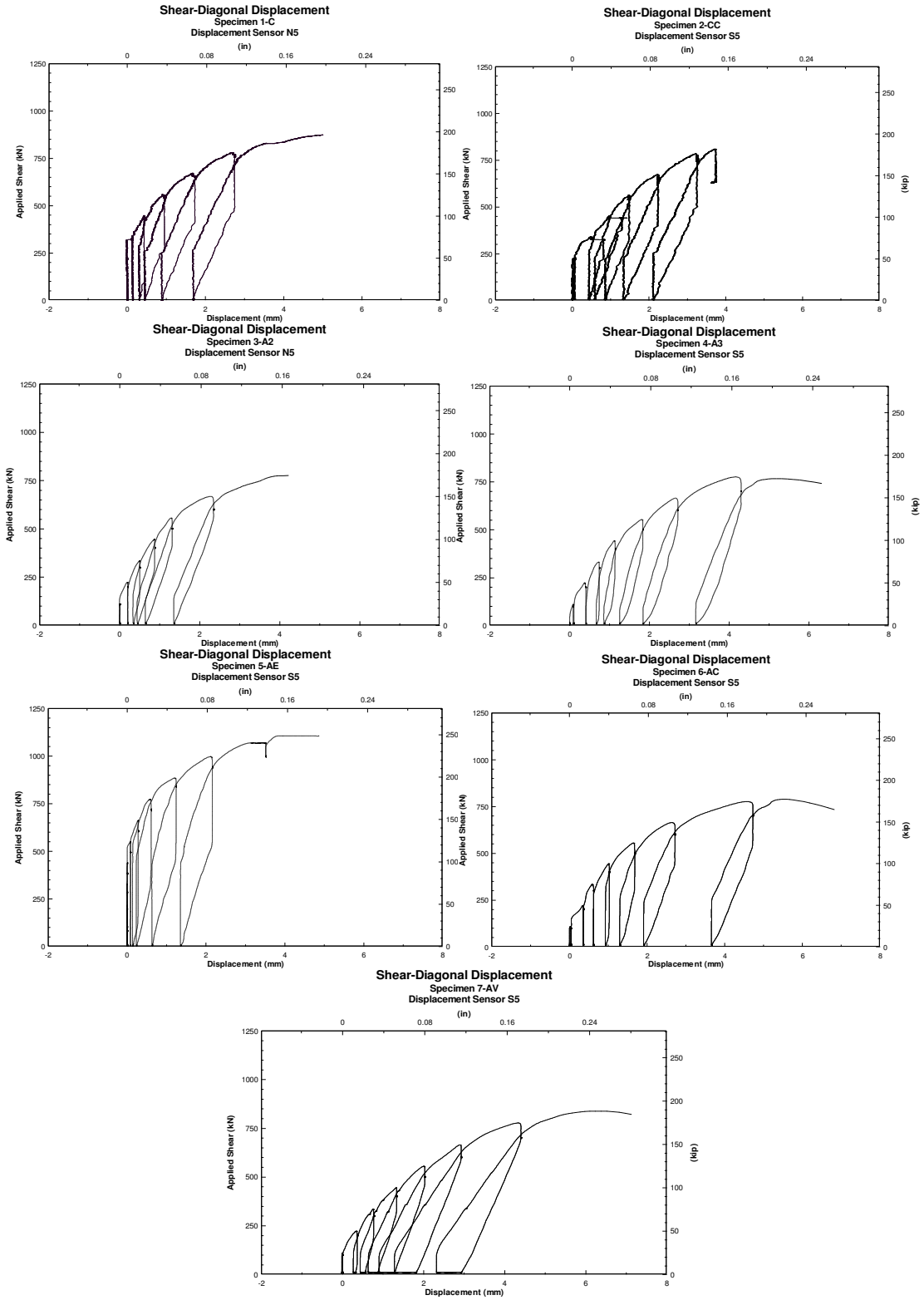

Fig. 3.5: Shear-diagonal displacement response near the failure section.

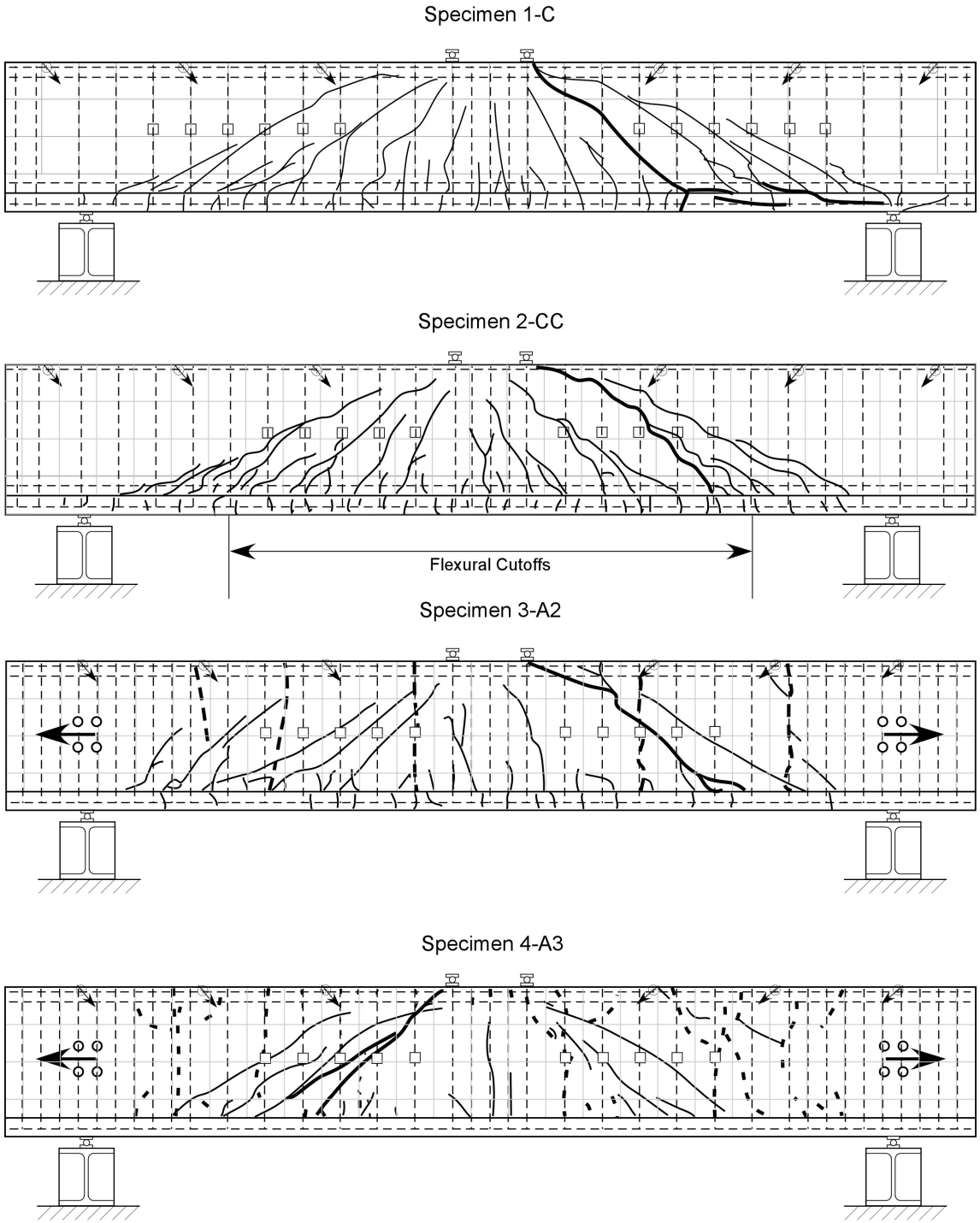

Fig. 3.6: Crack Pattern Locations on east face of specimens.

Fig. 3.6 (Continued)

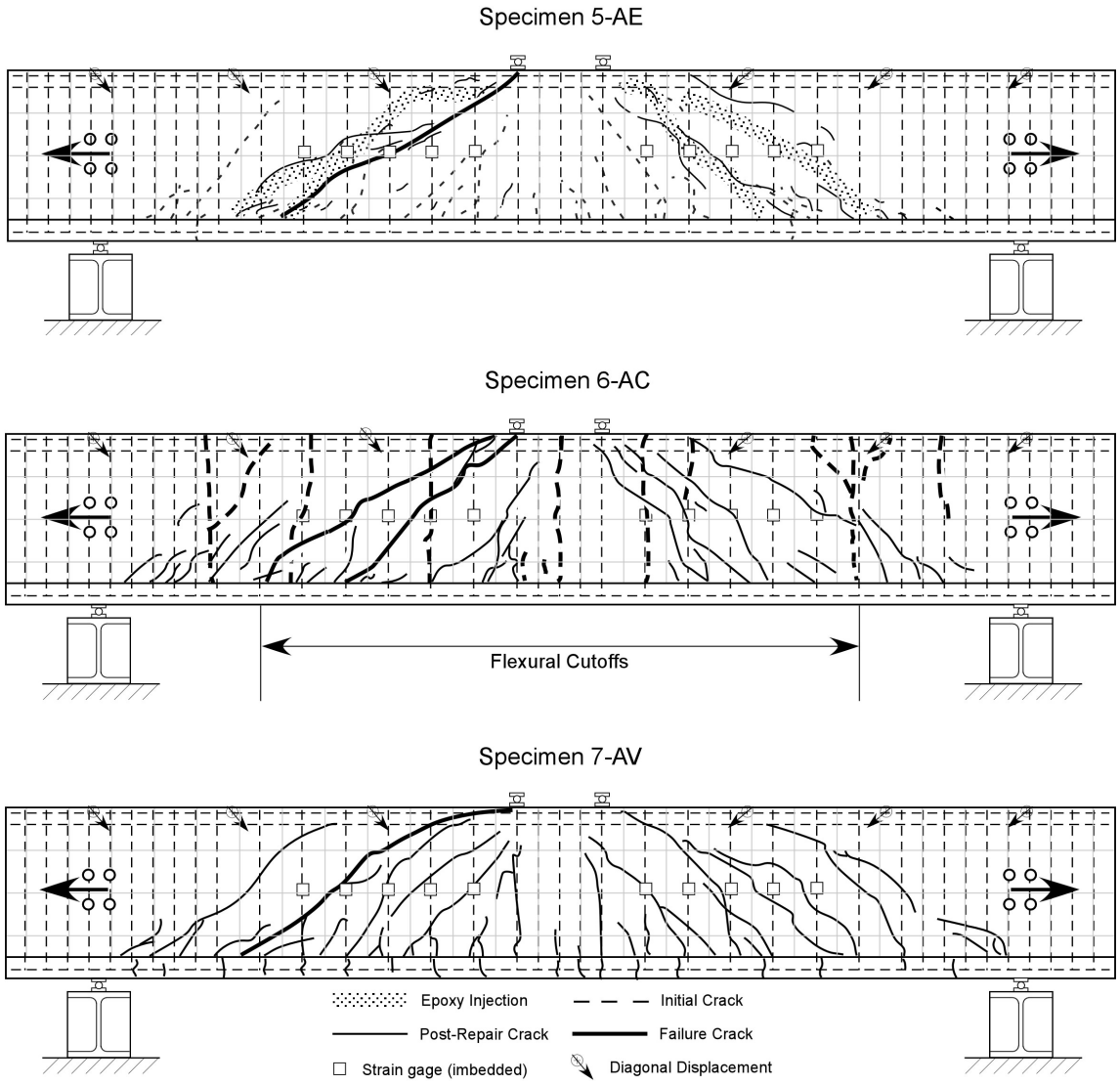

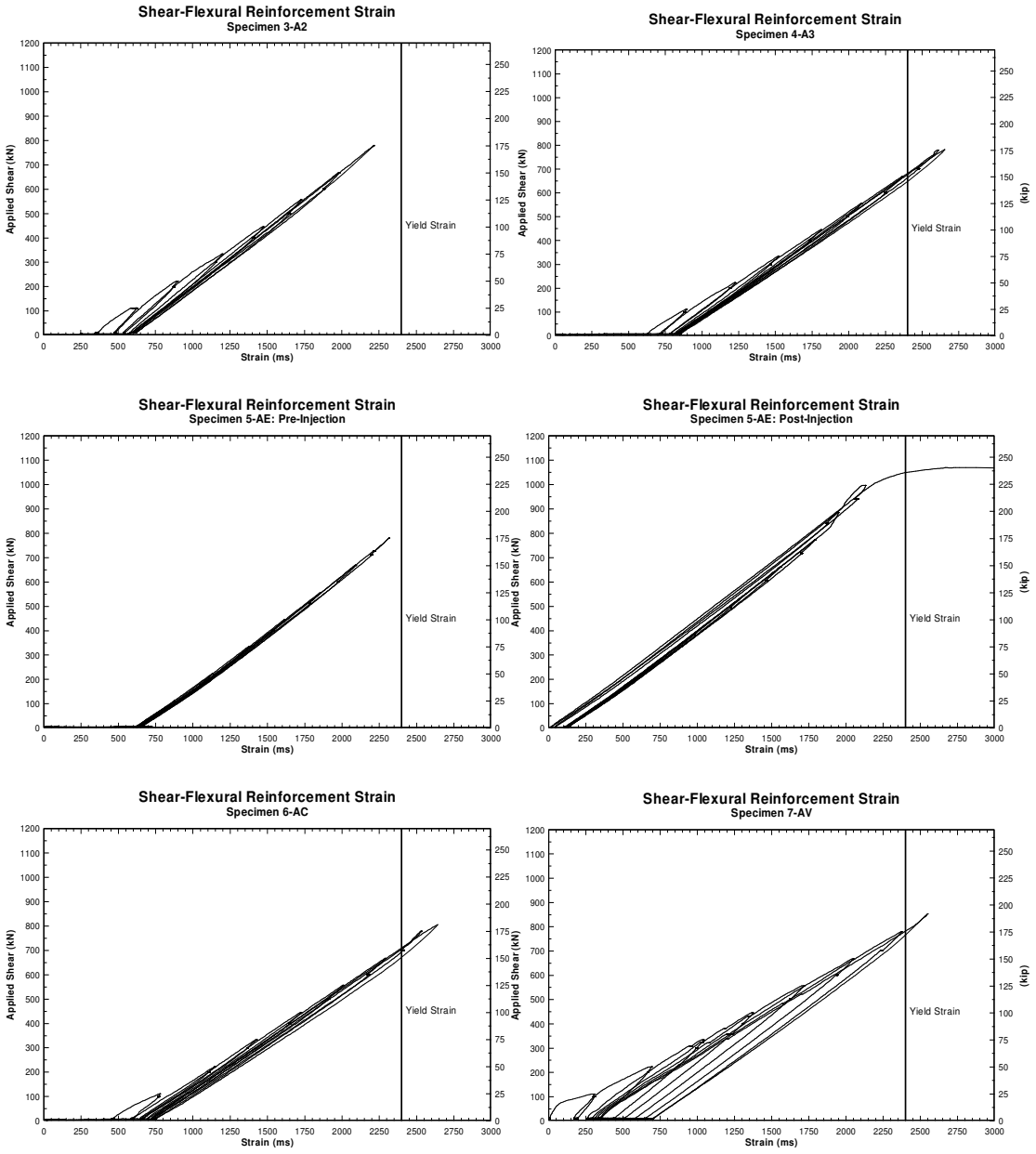

Fig. 3.7: Shear-midspan flexural strain response for axial specimens.

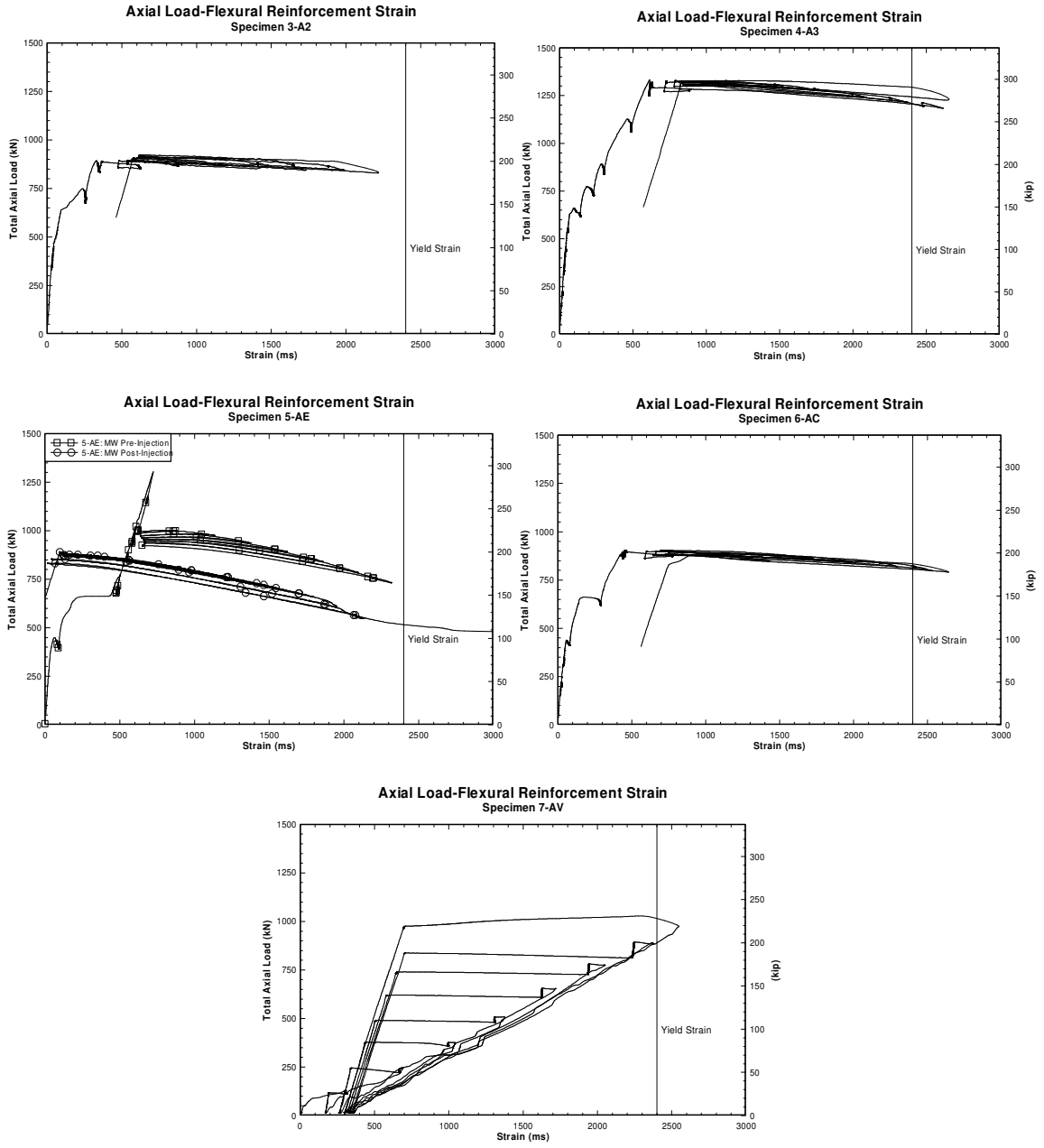

Fig. 3.8: Axial Load-midspan flexural strain response for axial specimens.

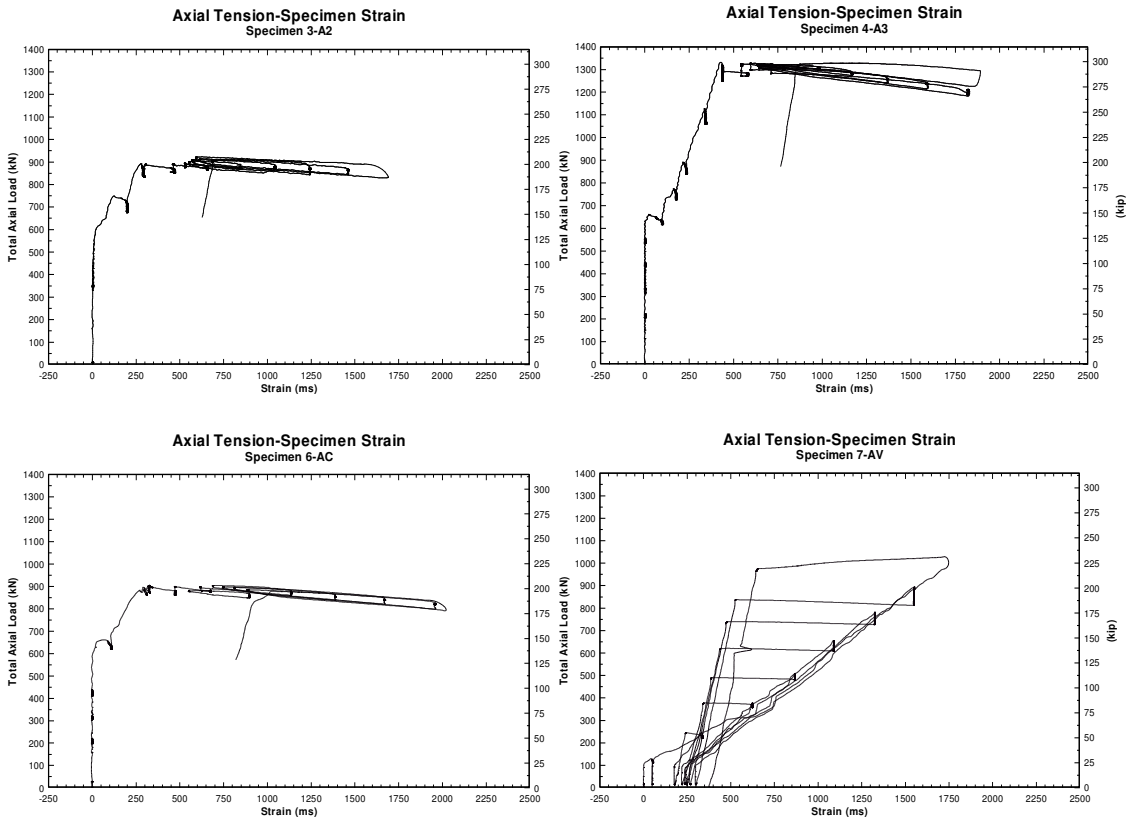

Fig. 3.9: Axial tension-specimen strain.

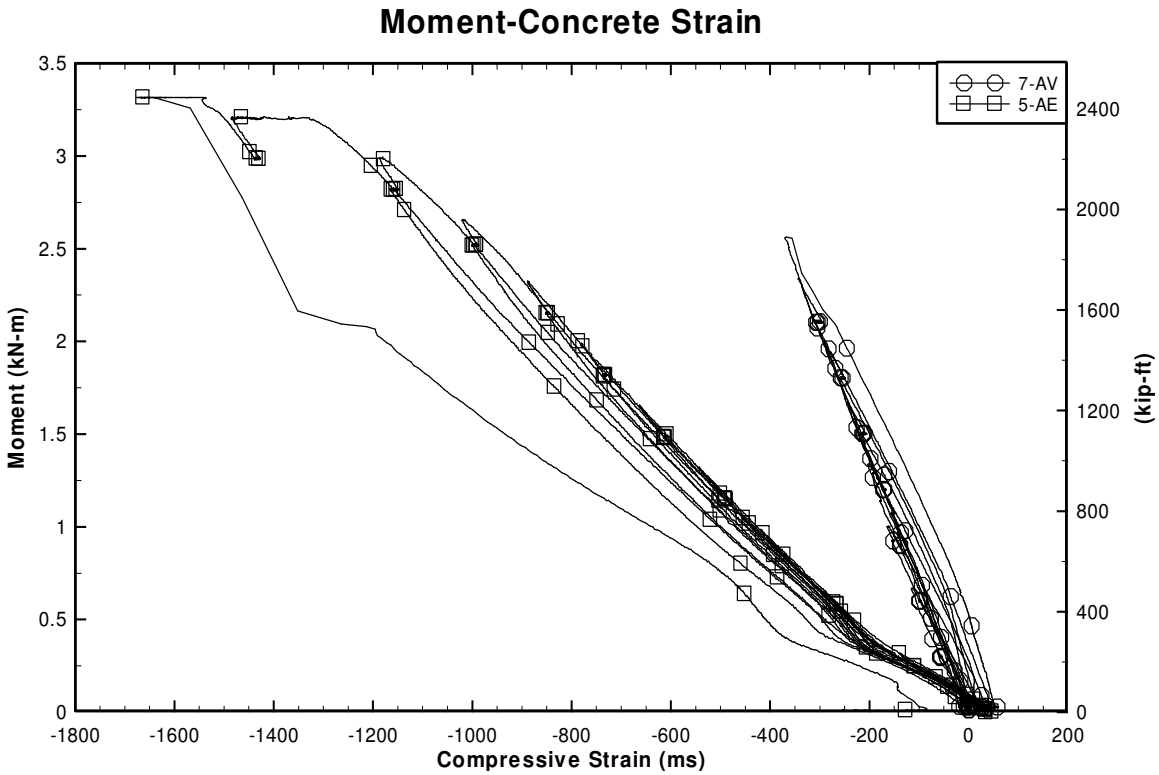

Fig. 3.10: Moment-concrete strain.

General Conclusion

Ten CRC girders built to reflect the design and construction practice of 1950's vintage RCDG bridges were tested to study the effects of epoxy injection and applied axial load to diagonal cracks on structural performance. Four specimens were epoxy injected, four specimens were axially tensioned, and two served as control specimens. Factors included constant and variable axial tension, flexural cutoff detailing, and epoxy injection under various imposed service loads. Based on the experimental observations and results, the following conclusions are presented:

- Capacity was only slightly increased by epoxy injection. The largest capacity increases were observed for specimens with the live load and externally applied axial tension (which was due principally to an unintended post-tensioning effect).
- Live loading during injection and curing of epoxy produced dynamic pressure fluctuations during the injection process and pumping of the epoxy within the diagonal cracks. Fine bubbles were identified in the epoxy matrix for cores taken after testing for the specimen with applied live loads, but these bubbles were not sufficient to diminish performance.
- Stiffness was improved and development of residual deformations was delayed by epoxy injection.
- Epoxy injection increased the load level required to form diagonal cracks in the stem.

- Injected diagonal cracks did not reopen, instead new cracks formed adjacent to the original injected cracks.
- Epoxy injection reduced service-level stirrup strains compared to un-injected diagonal cracks. This may reduce bond fatigue thereby slowing or preventing additional crack growth.
- Superimposed axial tension reduced member shear-flexure capacity and reduced overall member stiffness.
- Initially applied axial tension reduced the transverse force required to initiate diagonal cracking.
- Axial load applied simultaneously with transverse load further reduced the transverse force required to initiate diagonal cracking.
- Reinforcing steel terminated in the flexural tension region combined with axial tension did not significantly reduce shear-flexure capacity beyond that of axial tension alone, for the shear-compression failure modes observed. Member capacity may be further reduced when shear-tension failures occur.
- The combined effects of flexural cutoffs and axial tension reduced global member stiffness beyond that of axial tension alone.
- R2K overestimated shear-flexure capacity for specimens with axial tension force of 890 kN (200 kip) and underestimated capacity for the specimen with tension force of 1334 kN (300 kip).
- AASTHO-LRFD and ACI 318-05 underestimated specimen shear capacity for all axial tension forces considered in this study.

BIBLIOGRAPHY

AASHTO LRFR, American Association of State Highway and Transportation Officials, "Manual for Condition Evaluation and Load and Resistance Factor Rating (LRFR) of Highway Bridges," Washington, DC., 2003

AASHTO LRFD, American Association of State Highway and Transportation Officials, "Load Rating and Factored Design (LRFD) Bridge Design Specifications," Washington, DC., 2004

Abu-Tair, A. I., Rigden, S. R., and Burley, E., "The Effectiveness of the Resin Injection Repair Method for Cracked RC Beams," *The Structural Engineer*, V. 69, No. 19, Oct. 1991, pp. 335-341

ACI Committee 209, "Prediction of Creep, Shrinkage, and Temperature Effects in Concrete Structures," (ACI 209-R92), American Concrete Institute, Detroit, 1992, 47 pp.

ACI 318-05, "Building Code Requirements for Structural Concrete," American Concrete Institute, Farmington Hills, Michigan, 2005

ACI Committee 503, "Guide for the Selection of Polymer Adhesives with Concrete," *ACI Materials Journal*, V. 89, No. 1 Jan-Feb, 1992, pp. 90-105

ACI Committee 503, "Use of Epoxy Compounds with Concrete," (ACI 503R-93), *American Concrete Institute*, July 1993, 28 pp.

ACI Committee 224, "Causes, Evaluation, and Repair of Cracks in Concrete," (224.1R-93,) American Concrete Institute, Sept. 1993, 22 pp

ASTM C 39/C 39M-05, "Standard Test Method for Compressive Strength of Cylindrical Concrete Specimens," ASTM International, 2005, pp. 21-27.

ASTM C 617-98, "Standard Practice for Capping Cylindrical Concrete Specimens," ASTM International, 2005, pp. 1-5.

Basunbul, I. A., Gubati, A. A., Al-Sulaimani, G. J., and Baluch, M. H., "Repaired Reinforced Concrete Beams," *ACI Materials Journal*, V. 87, No. 4, July-Aug. 1990, pp. 348-354

Bentz, E., Repsonse 2000, University of Toronto, <http://www.ecf.utoronto.ca/~bentz/r2k.htm>.

Bentz, E., AASHTO Shear Calculator, University of Toronto

Bryant, A. H., and Vadhanavikkit, C., "Creep, Shrinkage-size, and Age at Loading Effects," American Concrete Institute Materials Journal, V. 84, No. 2, Mar.-Apr. 1987, pp. 117-123

Chung, H. W., "Epoxy-Repaired Reinforced Concrete Beams," *Journal of the American Concrete Institute,* V. 72, No. 5, May 1975, pp. 233-234

Chung, H. W., "Epoxy Repair of Bond in Reinforced Concrete Members," *Journal of The American Concrete Institute*, V. 78, No.1, Jan.-Feb. 1981, pp. 79-82

Comite' Euro-International du Be'ton, CEB-FIP Model Code 1990, Thomas Telford Services Ltd. London, 1993

El-Hawary, M., Al-Khaiat, H., Fereig, S., "Performance of Epoxy-repaired Concrete in a Marine Environment," *Cement and Concrete Research,* V. 30, No. 2, Feb. 2000, pp. 259-266

Emmons, P. H., Vaysburd, A. M., McDonald, J. E., "Concrete Repair in the Future Turn of the Century." *Concrete International: Design and Construction*, V. 16, No. 3, March 1994, pp.42-49

Higgins, C., Farrow, W III, C., Potisuk, T., Miller, T. H., Yim, S. C., Holcomb, G. R., Cramer, S. D., Covino, B. S., Bullard, S. J., Ziomek-Moroz, M., and Matthes, S. A., "SPR 326 Shear Capacity Assessment of Corrosion-Damaged Reinforced Concrete Beams," Oregon Department of Transportation, Salem, OR, 2003, 19 pp.

Higgins, C., Miller, T. H., Yim, S. C., Potisuk, T., and Robelo, M. J., "Research Project SPR 341: Remaining Life of Reinforced Concrete Beams with Diagonal-Tension Cracks," Oregon Department of Transportation, Salem, OR, April 2004, 110 pp.

Higgins, C., Miller, T. H., Rosowsky, D. V., Yim, S. C., Potisuk, T., Daniels, T. K., Nicholas, B. S., Robelo, M. J., Lee, A-Y., and Forrest, R. W., "Research Project SPR 350 SR 500-91: Assessment Methodology for Diagonally Cracked Reinforced Concrete Deck Girders," Oregon Department of Transportation, Salem, OR, Oct. 2004, 328 pp.

Hughes, B. P., and Mahmood, A. T., "Laboratory Investigation of Early Thermal Cracking of Concrete," American Concrete Institute Materials Journal, V. 85, No. 3, May-Jun 1988, pp. 164-171

Kuennen, T., "Taming Oregon's Cracked Bridges," *Better Roads,* V. 76, No. 4, April 2006, pp. 54-62

Li, Q., Duan, and Y., Wang, G., "Behaviour of Large Concrete Specimens in Uniaxial Tension," *Magazine of Concrete Research*, V. 54, No. 5, Oct. 2002, pp. 385-391

Nishibayashi, Shinzo, *et al.*, "Fatigue Performance of Reinforced Concrete Beams Repaired by Epoxy Resin Injection" *Transactions of the Japan Concrete Institute*. V. 8, 1986, pp.559-566

Ozaka, Y., Suzuki, M., "Shear Repair of Reinforced Concrete Beams and Effect of Repair by Epoxy Injection," Special Publication-*American Concrete Institute,* V. 93 Sept. 1986, pp.637-670

Popov, E. P., and Bertero, V. V., "Repaired R/C Members Under Cyclic Loading," *Earthquake Engineering and Structural Dynamics,* V. 4, No. 2, Oct.-Dec. 1975, pp. 129-144

Potisuk, T., and Higgins, C., "Field Testing and Analysis of CRC Girder Bridges," *Journal of Bridge Engineering*, ASCE, V. 12, No. 1, Jan.-Feb. 2007, pp. 53-63

Rigden, S. R., Burley, E., French, W. F., Abu-Tair, A. I., Dalziel, J., "The Use of Resin Injection to Repair an Impact-damaged Motorway Bridge," *Structural Engineer,* V. 73, No. 12, June 20, 1995, pp. 200-201

Rizkalla, S. H., Hwang, L. S., "Crack Prediction for Members in Uniaxial Tension," *Journal of the American Concrete Institute*, V. 81, No. 6, Nov.-Dec. 1984, pp. 572-579

Rooney, R. A., "Epoxy Resins as a Structural Repair Material," State of California Department of Public Works Division of Highways, <http://www.dot.ca.gov/hq/research/researchreports/1961-1963/63-23.pdf, Jan. 1963, pp. 15

Shash, A. A., "Repair of Concrete Beams-A Case Study," *Construction and Building Materials*, V. 19, No.1, Feb. 2005, pp. 75-79

Thanoon, Waleed A., Jaafar, M. S., Kadir, M. Razali A., Noorzaei, J., "Repair and Structural Performance of Initially Cracked Reinforced Concrete Slabs" *Construction and Building Materials,* V. 19, No. 8 Oct. 2005, pp.595-603

Tremper, B., "Repair of Damaged Concrete with Epoxy Resins," *Journal of the American Concrete Institute,* V. 32, No. 2, Aug. 1960, pp. 173-182

Tsiatas, G. C., "Durability Evaluation of Concrete Crack Repair Systems," *Transportation Research Record*, No. 1795, 2002, pp.82-87

Williams, Grahme T., "Investigation of the Fatigue Behavior of Diagonally-Cracked CRC Deck-Girders Repaired with CFRP" Oregon State University, 2006

NOTATION

A_g = gross section of area

A_{ps} = area of prestressing steel

A_s = area of nonprestressed tension reinforcement

A_v = area of transverse reinforcement within distance of s

b_v, b_w = width of web

d = distance from compression face to centroid of tension reinforcement

d_v = distance between the flexural tension and compression resultants

f'_c = concrete compressive strength

E_s = modulus of elasticity of reinforcing bars

E_p = modulus of elasticity of prestressing tendons

f_{po} = a parameter taken as modulus of elasticity of prestressing tendons multiplied by the locked-in difference in strain between the prestressing tendons and the surrounding concrete

F_u = steel ultimate strength

F_y = steel yield strength

F_{yl} = yield strength of longitudinal reinforcement

F_{yt} = yield strength of transverse reinforcement

L = length

M_u = factored moment at the section

N_u = applied axial force taken as tensile if positive

s = spacing of transverse reinforcing bars

V_{app} = total applied experimental shear (sum of V_{exp} and V_{DL})

V_{exp} = experimental shear

V_{DL} = member dead load contribution to applied experimental shear

V_n = nominal shear resistance

V_c = nominal shear resistance provided by tensile stresses in the concrete

V_p = component in the direction of the shear of the effective prestressing force

V_s = shear resistance provided by shear reinforcement

V_u = factored shear force at section

α = angle of inclination of transverse reinforcement to longitudinal axis

β = factor relating effect of longitudinal strain on the shear capacity of concrete

θ = angle of inclination of diagonal compressive stresses